# Photocatalytic reduction of CO2 by CO co-feed combined with photocatalytic water splitting in a novel twin reactor

Elsevier Editorial System(tm) for Energy Conversion and Management

Manuscript Draft

Manuscript Number: ECM-D-16-00352R1

Title: Photocatalytic reduction of CO2 by CO co-feed combined with photocatalytic water splitting in a novel twin reactor

Article Type: Original research paper

Section/Category: 3. Clean Energy and Sustainability

Keywords: twin reactor; CO2 reduction; water splitting; photocatalysis; methanol; sun light intensity

Corresponding Author: Prof. Lijun Yang, Ph. D.

Corresponding Author's Institution: North China Electric Power University

First Author: Shang Li

Order of Authors: Shang Li; Lijun Yang, Ph. D.; Oluwafunmilola Ola; Mercedes Maroto-Valer; Xiaoze Du; Yongping Yang

Abstract: As a promising way to control greenhouse gas emission and alleviate global energy shortage, photocatalytic reduction of carbon dioxide attracts more attentions in recent years since it can produce fuels efficiently with the combination of H2 through water splitting. In this work, a computational model which characterizes the photocatalytic reduction of carbon dioxide by CO co-feed in a novel twin reactor is developed with three subsidiaries of chemical reaction kinetics, gas-liquid mass transfer, and transient sun light intensity distribution. Thanks to previous experimental work as the reliable verification for the numerical simulation, the variations of the CH3OH concentration with the CO/CO2 ratio of gas mixture, pressure and temperature are obtained and analyzed. The results show that the carbon in CO can form CH3OH directly, however the excessive CO will react with HCOOCH3 to form CH3CHO, which results in a reduced CH3OH concentration. Besides, the CH3OH concentration subsequently increases as the temperature and pressure increase, and the CH3OH product and reaction rate vary widely with time due to the changing sun light intensity during the day.

Dear Editor

Thanks for your comments and suggestions on our manuscript. Those comments are all valuable and very helpful for revising and improving our paper, as well as important for guiding our researches. We have modified the manuscript accordingly and seriously. Detailed corrections are listed in the response file and the revised manuscript.

Sincerely yours

Corresponding author: Lijun Yang

Email: yanglj@ncepu.edu.cn

School of Energy Power and Mechanical Engineering,
North China Electric Power University,
Beijing 102206, China

**Graphical Abstract (for review)**

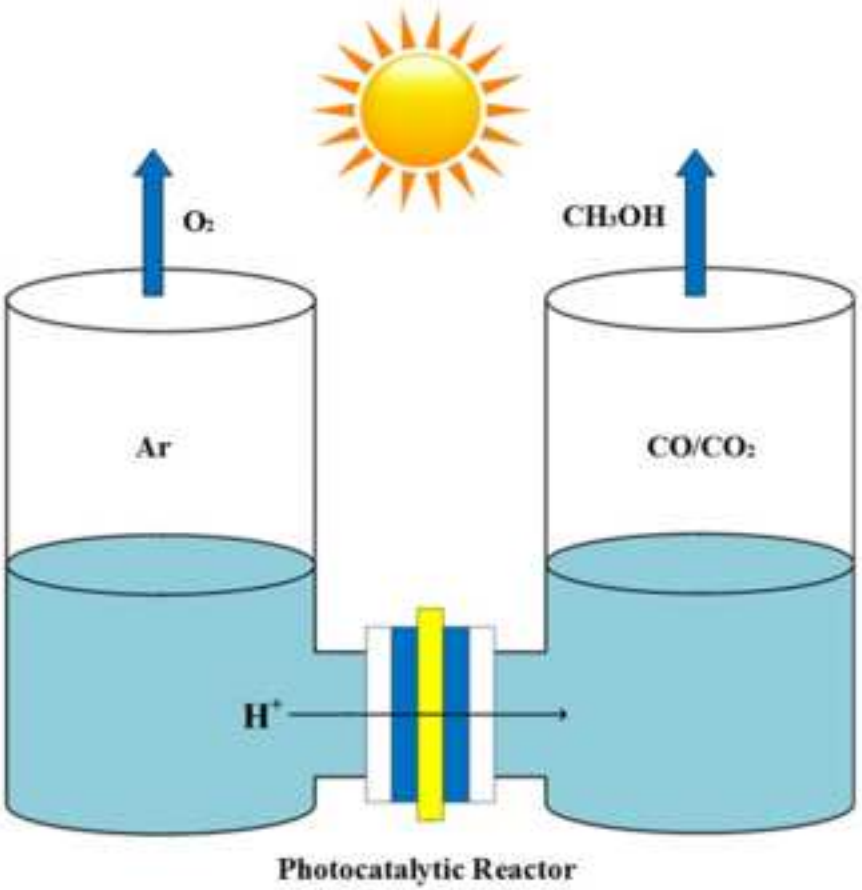


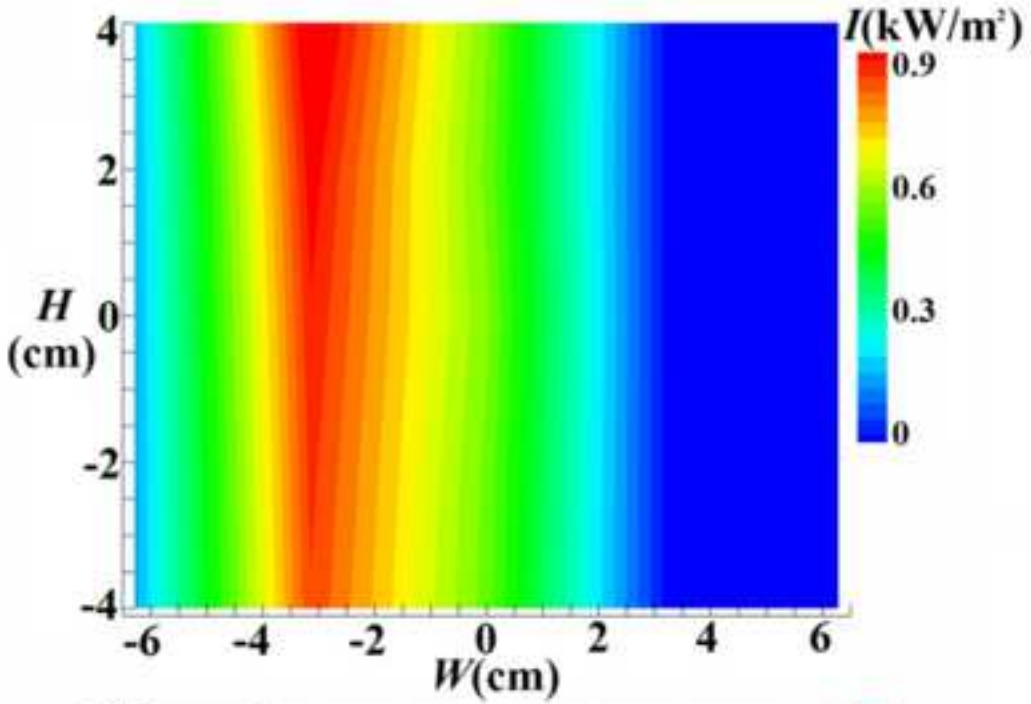


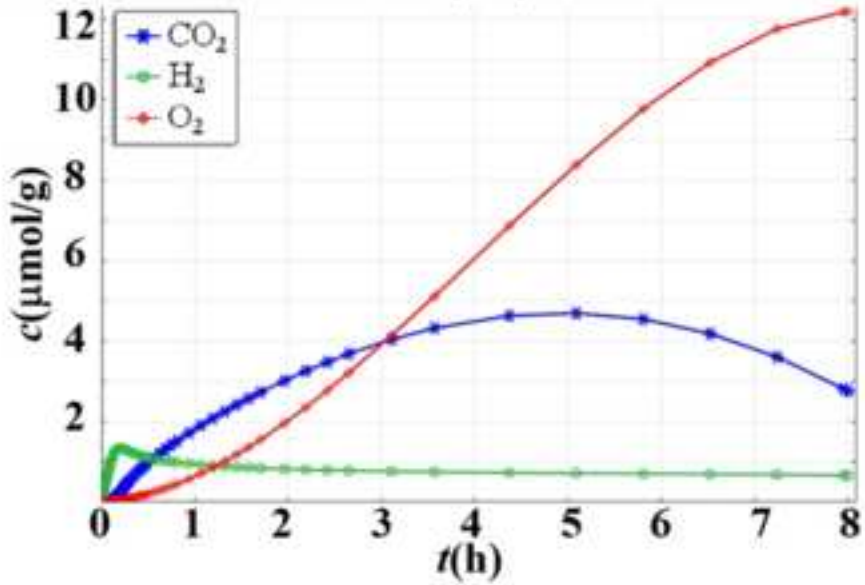

## Research Highlights

Photocatalytic $CO_2$ reduction combined with $H_2$ through water splitting is studied.

The carbon in CO can form $CH_3OH$ directly, so can increase $CH_3OH$ concentration.

Excessive CO will react with $HCOOCH_3$, resulting in a reduced $CH_3OH$ concentration.

$CH_3OH$ concentration increases with increasing the reactor temperature and pressure.

$CH_3OH$ product and reaction rate vary widely with time due to changing sun light.

# Photocatalytic reduction of $CO_2$ by CO co-feed combined with photocatalytic water splitting in a novel twin reactor

Shang Li[1], Lijun Yang*[1], Oluwafunmilola Ola*[2], Mercedes Maroto-Valer[2], Xiaoze Du[1], Yongping Yang[1]

*1. Key Laboratory of Condition Monitoring and Control for Power Plant Equipments of Ministry of Education,*

*School of Energy Power and Mechanical Engineering, North China Electric Power University, Beijing 102206, China*

*2. Centre for Innovation in Carbon Capture and Storage (CICCS),*

*School of Engineering and Physical Sciences, Heriot-Watt University, Edinburgh, EH14 4AS, UK*

**ABSTRACT**

As a promising way to control greenhouse gas emission and alleviate global energy shortage, photocatalytic reduction of carbon dioxide attracts more attentions in recent years since it can produce fuels efficiently with the combination of $H_2$ through water splitting. In this work, a computational model which characterizes the photocatalytic

* Corresponding author: Lijun Yang. Tel: +86 10 61773373; Fax: +86 10 61773877. *E-mail address:* yanglj@ncepu.edu.cn

Oluwafunmilola Ola. Tel: +44 (0) 131 451 4737. *E-mail address:* O.O.Ola@hw.ac.uk

reduction of carbon dioxide by CO co-feed in a novel twin reactor is developed with three subsidiaries of chemical reaction kinetics, gas-liquid mass transfer, and transient sun light intensity distribution. Thanks to previous experimental work as the reliable verification for the numerical simulation, the variations of the $CH_3OH$ concentration with the $CO/CO_2$ ratio of gas mixture, pressure and temperature are obtained and analyzed. The results show that the carbon in CO can form $CH_3OH$ directly, however the excessive CO will react with $HCOOCH_3$ to form $CH_3CHO$, which results in a reduced $CH_3OH$ concentration. Besides, the $CH_3OH$ concentration subsequently increases as the temperature and pressure increase, and the $CH_3OH$ product and reaction rate vary widely with time due to the changing sun light intensity during the day.

***Key words*****:** twin reactor, $CO_2$ reduction, water splitting, photocatalysis, methanol, sun light intensity

33 **Nomenclature**

| | | |
|---|---|---|
| $c$ | concentration | $mol \cdot m^{-3}$ |
| $D$ | diffusion coefficient | $m^{2} \cdot s^{-1}$ |
| $I$ | light intensity | $W \cdot m^{-2}$ |
| $k$ | kinetic rate constant | $m^{4} \cdot s^{-1} \cdot mol^{-2}$ |
| $L$ | reactor height | mm |
| $M$ | molecular weight | $g \cdot mol^{-1}$ |
| $p$ | pressure | Pa |
| $r$ | reaction rate | $mol \cdot m^{-3} \cdot s^{-1}$ |
| $R$ | radius | mm |
| $t$ | time | s |
| $T$ | temperature | K |
| $V$ | molar volume | $cm^{3} \cdot mol^{-1}$ |
| $N$ | mass transfer rate | $mol \cdot m^{-2} \cdot s^{-1}$ |
| $K$ | mass transfer coefficient | $s \cdot mol \cdot kg^{-1} \cdot m^{-1}$ |
| $H$ | Henry constant | $Pa \cdot m^{3} \cdot mol^{-1}$ |
| $V$ | ionic strength | $mol \cdot m^{-3}$ |
| $E$ | electric field intensity | $V \cdot m^{-1}$ |
| $z$ | ionic valence | |
| $h$ | solubility coefficient | |

| | |
|---|---|
| $X$ | sun unit vector |
| $Y$ | sun unit vector |
| $Z$ | sun unit vector |
| $m$ | energy coefficient |
| $Rf$ | reflectivity |
| $Tr$ | transmissivity |
| $Ab$ | absorptivity |
| $n$ | refractivity |
| $L$ | latitude |
| $Day$ | day of year |
| $Hr$ | local solar time |

Greek letters

| | | |
|---|---|---|
| $\delta$ | film thickness | mm |
| $v$ | chemical calculated number | |
| $\rho$ | density | $kg \cdot m^{-3}$ |
| $\varphi$ | correction coefficient of Henry constant | |
| $\psi$ | proportional coefficient | S |
| $\omega$ | hour angle | |
| $\delta$ | declination | |
| $\alpha$ | solar altitude | |

| | |
|---|---|
| $\gamma$ | solar azimuth |

Subscript and superscript

| | |
|---|---|
| *A* | material |
| *B* | material |
| *F* | material |
| *O* | material |
| *a* | chemical calculated number |
| *b* | chemical calculated number |
| *f* | chemical calculated number |
| *o* | chemical calculated number |
| *L* | liquid phase |
| *G* | gas phase |
| *j* | number of reaction |
| *i* | number of reactant or ion |
| *m* | interface |
| *s* | sun |
| *x* | carbon source from carbon dioxide |
| *y* | carbon source from carbon monoxide |

35

## 1. Introduction

Since fossil fuels dominate more than 85% of energy consumption all over the world at the status quo, the rapid depletion has concentrated the growing concerns on the global energy crisis and an increasing carbon dioxide ($CO_2$) emission, which motivates researchers exploring the $CO_2$ reduction and utilization[1-5]. In the past decades, the conversion of $CO_2$ to value-added chemicals and renewable fuels has been investigated by various methods such as thermal conversion, plasma conversion and photoreduction[6]. Among various technologies of energy conservation and emission reduction[7-9], the photocatalytic $CO_2$ reduction into hydrocarbon fuels is a promising and eco-friendly method to prevent the increasing of greenhouse gases and depletion of fossil resources[5, 10, 11]. Since the first demonstration in 1979 by Inoue et al.[12], the approach of photocatalytic $CO_2$ reduction has received increasing attentions [13-15].

For the traditional photo-technology, $CO_2$ can be reduced by water ($H_2O$) to CO, $CH_4$, HCOOH, HCHO and $CH_3OH$ over semiconductor materials such as $TiO_2$, ZnO, $WO_3$, SiC, CdS, and GaP[16-19]. However, $CO_2$ is hardly reducible since $H_2O$ is a weak reductant. What's worse, the hydrocarbon products can be easily oxidized, which results in a low output ratio of hydrocarbons unexpectedly. In recent years, the technology of hydrogen production from photocatalytic water splitting has achieved a rapid progress [20, 21]. In 1987, Thampi et al.[22] reported that under the action of

$TiO_2$ nanoparticles catalyst, $CH_4$ was produced from the gas mixture of $H_2$ and $CO_2$ with the production rate of about 116μL/h. And in 2007, Lo et al.[23] confirmed that the $CO_2$ photoreduction was improved by a mixture of $H_2$ and $H_2O$ compared with that using solely $H_2$ or $H_2O$. Many studies on $CO_2$ hydrogenation to yield organics have been reported, which provide a theoretical basis for the chemical reactions of photocatalytic reduction of carbon dioxide with the combination of $H_2$ through water splitting. Twin reactor system can combine the water splitting with $CO_2$ reduction because the reducibility of $H_2$ is better than $H_2O$, so the $CO_2$ photo-reduction with $H_2$ through water splitting is more viable to produce fuels at a higher yield rate [11], as it has also been experimentally investigated in previous studies [24-26].

Twin reactor usually consists of two components for photocatalytic water splitting and photocatalytic $CO_2$ reduction, which are divided by an ion exchange unit. $H^+$ from water splitting is directly used to perform the $CO_2$ photo-hydrogenation with the participation of the light at the room temperature. The conversion of $CO_2$ into hydrocarbons is feasible from the thermodynamic viewpoint. For instance, the photoreduction of $CO_2$ to produce $CH_3OH$ can be represented by five possible reactions as listed in Table 1. The enthalpies ($\Delta H^0$) of all the five reactions are negative at room temperature, which proves that the reactions are exothermic. The Gibbs free energies ($\Delta G^0$) of the reactions (1), (4) and (5) are negative, meaning that the reactions are spontaneous, equilibrium favorable. Moreover, although the $\Delta G^0$ of

the reactions (2) and (3) are positive, meaning that they are thermodynamically not spontaneous, those values are still much lower than that of water splitting ($\Delta H^0$= 285.8 kJ/mol; $\Delta G^0$ = 237.1 kJ/mol). Hence, the photocatalysts can convert photon energy into chemical energy accompanied by this slightly positive change in the Gibbs free energy[25]. The combination of photocatalytic $CO_2$ reduction with water splitting in the twin rector presents a better performance than the $CO_2$ reduction by $H_2O$, and prevents the oxygenation of hydrocarbon products.

CO was considered as a co-feed to enhance the production efficiency of $CH_3OH$, and a certain amount of CO mixed with the reaction gases can promote $CH_3OH$ production under the same conditions because CO is thermodynamically more favorable as compared to the $CO_2$. However, due to the limitation of experimental conditions, it did not address how the CO affects the methanol production. When the reaction gas is pure CO, $CH_3OH$ cannot be produced, which was not clarified in detail by previous studies. Other operating conditions such as the pressure and temperature in the twin reactor, which are crucial to the photocatalytic reduction of $CO_2$, were also not deeply investigated. What's more, there are few related studies about the sun light effect on the photocatalytic $CO_2$ reduction in twin reactors, since most of the experiments were carried out in an indoor environment with the artificial light instead of natural sources. Adopting the software SOLTRACE in this work, the principle of CO effect on the $CH_3OH$ production and the impacts of operation conditions on the

conversion efficiency from $CO_2$ to $CH_3OH$ in the twin reactor are deeply investigated by unveiling the sun light distribution as well as the photocatalytic $CO_2$ reduction mechanism. It can be of benefit to the optimal design and operation of twin reactors by investigating the photocatalytic reduction of $CO_2$ by CO co-feed combined with photocatalytic water splitting.

## 2. Model development

### *2.1 Physical model*

The physical model of the twin reactor can be simplified as Fig.1, which has been described in detail and experimentally investigated in some of the photocatalytic characteristics [24-26]. With a Nafion membrane for segregation, 0.15 g of $Pt/CuAlGaO_4$ and 0.15 g of $Pt/SrTiO_3$:Rh in 2mM $FeCl_2$ were placed in the $CO_2$ reduction reactor solution, while 0.30 g of commercial $WO_3$ in 2mM $FeCl_3$ solution were put in the water splitting reactor. In the novel twin reactor, one of the key components is the modified Nafion membrane that allows not only the transport of hydrogen ions, but also the exchange of the electron mediators ($Fe^{2+}/Fe^{3+}$). The electron is shuffled via the electron mediator ($Fe^{2+}/Fe^{3+}$) through membrane. The mass and charge balances are kept concurrently by the diffusion of $H^+$ through the membrane[27]. The pH of the solution is 2.6 (adjusted by adding sulfuric acid) and the volume of each compartment of the twin reactor is 225 mL. The $H^+$ generated by $H_2O$ splitting goes through the Nafion membrane and forms $H_2$, which reacts with

$CO_2$ to produce organic compounds. In this work, the multi-physics coupling software is used to simulate the above process with the following necessary assumptions, based on which the model can be well simplified without introducing unexpected errors.

1) Since the driving force of the photoreaction originates from the light energy but not the thermal energy (i.e. molecular kinetics at high temperatures) in the traditional catalytic reaction, most photoreactions work at about the room temperature. As a result, the thermodynamic effects of the reactions at various temperatures can be ignored because of the extremely weak provoking energy in the photocatalysis.
2) Thanks to the magnetic stirrer in the experiment for the uniform catalyst distribution in the solution, the reaction rate is assumed to be a function of the time rather than the location.
3) Since CO and $CO_2$ are free from liquidation at the room temperature and atmospheric pressure, the mixture can be seen as an ideal gas so as to easily calculate the partial pressure based on the ideal gas equation. Besides, the chemical process at the interface of the gas and liquid is not taken into account.
4) The effects of the catalyst surface topography, concentration, band gap, and absorption or desorption existing on the surface of catalyst particles are ignored.
5) The chemical reactions in the twin reactor take the following forms, which are regarded as single step reactions [25].

$$h\nu \xrightarrow{UV,photocatalyst} h^+ + e^-$$

$$H_2O + 2h^+ \xrightarrow{UV,photocatalyst} 2H^+ + \frac{1}{2}O_2$$

$$2H^+ + 2e^- \xrightarrow{UV,photocatalyst} H_2$$

$$CO_2 + 6H^+ + 6e^- \xrightarrow{UV,photocatalyst} CH_3OH + H_2O$$

$$CH_3OH + CO \xrightarrow{UV,photocatalyst} HCOOCH_3$$

$$CH_3OH + CO_2 + 2H^+ + 2e^- \xrightarrow{UV,photocatalyst} HCOOCH_3 + H_2O$$

$$HCOOCH_3 + CO \xrightarrow{UV,photocatalyst} CH_3CHO + CO_2$$

$$HCOOCH_3 + 4H^+ + 4e^- \xrightarrow{UV,photocatalyst} CH_3OH$$

$$H_2O + CO \xrightarrow{UV,photocatalyst} H_2 + CO_2$$

With the aforementioned equations, the inferior middle processes are reasonably ignored for clearly uncovering the chemical mechanism from the reactants to products.

*2.2 Chemical reaction kinetics model*

For the chemical reaction aA+bB=fF+oO under constant volume conditions, the reaction rate can be expressed as follows:

$$r = -\frac{1}{a}\frac{dc_A}{dt} = -\frac{1}{b}\frac{dc_B}{dt} = \frac{1}{f}\frac{dc_F}{dt} = \frac{1}{o}\frac{dc_O}{dt} \quad (1)$$

When the reaction is an elementary reaction, the above formula can be written as:

$$r = kc_A{}^a c_B{}^b \quad (2)$$

Where $k$ is the reaction rate constant.

In previous studies, it has been noticed that the photocatalytic reaction rate follows a power law expression of the light intensity[28]. By experimental studies, Herrmann suggested that the reaction rate is proportional to the light intensity at low light

intensities, and when the light intensity is high, the reaction rate is proportional to the square root of the light intensity [29]. According to the work of Wang et al., the photocatalytic reaction rate was considered proportional to the n-th power of the light intensity[17], where n is a factor to describe the reaction rate dependency on light irradiance. The higher n value of the reactor represents that the incident photons can be more effectively utilized for photocatalytic reactions[30]. Therefore, the reversible catalytic reaction rate equation can be written with the following form:

$$r_j = I^m \left( k_j \prod_{i=1} c_i^{\nu_i} \right) \tag{3}$$

Where $r_j$ is the reaction rate, $k_j$ is the kinetic rate constant, $c_i$ is the concentration, $\nu_i$ is the chemical calculated number, $I$ is the light intensity, $m$ is the energy coefficient.

*2.3 Mass transfer model*

Many physical models, such as two-film, Higbie penetration, Danckwerts surface renewal and turbulent mass transfer theories, all formerly clarified the process of gas-liquid mass transfer. With two-film theory adopted in this work, a static film on each side of the gas-liquid interface is assumed as the gas membrane and liquid membrane. Moreover, the mass transfer rate of gas-liquid interphase depends on the diffusion rate of gas and liquid membranes.

$$N = \frac{D_G}{RT\delta_G}(p_G - p_m) = \frac{D_L}{\delta_L}(c_m - c_L) \tag{4}$$

Where $N$ is the mass transfer rate, $D_G$ and $D_L$ are the diffusion coefficients of components in gases and liquids respectively. $\delta_G$ and $\delta_L$ are the gas and liquid film thicknesses, which are about 0.1mm according to the experiment. $c_m$ and $p_m$ represent

the concentration and partial pressure at the interface of the membranes. $p_G$ is the partial pressure of components in gas phase while $c_L$ is the concentration of components in liquid phase. $R$ is the perfect gas constant and $T$ is temperature.

By eliminating the interface concentration $c_m$ and the interface pressure $p_m$ in the above formula, the mass transfer rate is expressed as:

$$N = K_G(p_G - p^*) = K_L(c^* - c_L)$$
$$p^* = Hc_L; c^* = \frac{p_G}{H} \tag{5}$$

Where $p^*$ is the partial pressure in equilibrium with $c_L$, $c^*$ is the concentration in equilibrium with $p_G$, $H$ is the Henry constant, $K_G$ and $K_L$ represent gas phase total mass transfer coefficient and liquid phase total mass transfer coefficient:

$$K_G = \frac{1}{\frac{RT\delta_G}{D_G} + \frac{H\delta_L}{D_L}}$$
$$K_L = \frac{1}{\frac{RT\delta_G}{HD_G} + \frac{\delta_L}{D_L}} \tag{6}$$

When the solution contains electrolytes, electrolyte ions will reduce the solubility of gases[31]. The Henry constant of gas in pure $H_2O$ is different from that in the electrolyte solution, hence the correction coefficient of Henry constant $\varphi$ has been introduced in the research of Ueyama and Hatanaka [31]:

$$H = \varphi H^0$$
$$\lg \varphi = \sum h_i V_i \tag{7}$$

$H^0$ and $H$ are Henry constants for the gas in the water and electrolyte, respectively. $V_i$ is the electrolyte ionic strength calculated by Eq.(8) as followed, and $h_i$ is the reduced coefficient of solubility caused by electrolyte, which is calculated by $h=h^+ + h^- + h^*$. $h^+$,

$h^-$, $h^*$ are influenced by the positive and negative ions, and the dissolved gases.

$$V_i = \frac{1}{2}\sum c_j z_j^{\ 2} \tag{8}$$

Where, $c_j$ is the ion concentration, $z_j$ is the ion valence.

The electrolytes in the system are $H^+$, $Fe^{2+}$, $Fe^{3+}$, $Cl^-$ and $SO_4^{2-}$ according to the related experiments.

As the physical model introduced above, the pH which has an impact on gas dissolution process, is set as 2.6 (adjusted by adding sulfuric acid) of the solution. In this work, $H^+$ is considered with the same electrolyte as $Fe^{2+}$, $Fe^{3+}$ and $Cl^-$, so the pH effects on the solubility of $CO_2$ are illustrated by the correction coefficient $\varphi$.

Diffusion coefficients of $CO_2$ in the mixed gas and the solution can be calculated according to the following formula [32, 33]:

$$\begin{aligned} \log D_L &= -8.1764 + \frac{712.5}{T} - \frac{2.591\times10^5}{T^2} \\ D_G &= \frac{435.7T^{3/2}}{P(V_A^{1/3}+V_B^{1/3})^2}\sqrt{\frac{1}{M_A}+\frac{1}{M_B}} \end{aligned} \tag{9}$$

Where $A$, $B$ are two kinds of gas in the reactor, $p$ is the total pressure, $T$ is the temperature in the reactor and equals to 293K and $M$ is the molar mass of the gas. $V$ is the molar volume with the constant of 22.4 L/mol, due to the fact that the $CO_2$ and CO are ideal gases in the reactor.

*2.4 Sun light model*

Since the photocatalytic $CO_2$ reduction cannot work without sun light input in the twin reactor, most of the experiments were carried out in an indoor environment with

the artificial light for substitute. Unfortunately, few related studies emphasized on the sun light distribution. While in this work, with the software SOLTRACE based on the theory from Spencer and Murty[34], the sun light distribution is obtained and analyzed for its optical performance, which is highly affected by the light diffusion as a key factor that can be predicted by setting up accurate parameters in SOLTRACE.

The angular intensity distribution and position of the light together define the natural energy source, and in Beijing (northern latitude 40°5', east longitude 116°16'), the 200nd day during the year with the maximum sun declination is usually selected for sunlight acquisition. Although the Gaussian and Pillbox apparatus can together determine the sun shape, it cannot represent the real sunlight condition due to the complex atmospheric factors as well as inevitable errors from the optical equipment. Since the Gaussian leads to an obviously higher error than pillbox, it is dismissed in this paper. The sunlight position ($X_s$, $Y_s$, $Z_s$) can be calculated by latitude ($L$: +N, -S), day of year (*Day*) and local solar time (*Hr*) as follows.

$$\begin{aligned} X_s &= sin\gamma_s cos\alpha_s \\ Y_s &= sin\alpha_s \\ Z_s &= cos\gamma_s cos\alpha_s \end{aligned} \tag{10}$$

Where $\alpha_s$ is the solar altitude and $\gamma_s$ is the solar azimuth, which can be obtained by the following form.

$$\begin{aligned} \alpha_s &= \sin^{-1}(\cos L \cos\delta \cos\omega + \sin L \sin\delta) \\ \gamma_s &= \cos^{-1}[\frac{\sin\alpha_s \sin L - \sin\delta}{\cos\alpha_s \cos L}] \end{aligned} \tag{11}$$

Where $\omega$ is the hour angle, $\omega$=15(*Hr*-12). *Hr* is the local solar time, which is set from 8:00 to 16:00. $\delta$ is the declination, $\delta$= 23.45sin (360(284+*Day*)/365). *Day* is set as 200, implying the maximum sun declination, and *L* as 40°5', representing the latitude of Beijing.

Optical properties can be obtained from the movement of rays when they hit the surfaces. According to the experiment of Chen et al.[25], the body of the reactor is made of glass which can be treated as fully transparent, so the absorptivity is set to 0. The reflectivity and the transmissivity of the twin reactor can be obtained by the following forms.

$$Rf = \frac{(n_1 - n_2)}{(n_1 + n_2)} \qquad (12)$$
$$Rf + Tr = 1$$

Where *Rf* is reflectivity, *Tr* is transmissivity, *n* is refractivity that can be obtained from the relevant literature. In addition, due to the effect of the element surface shape on ray direction, surface slope error and surface specularity can be included, which together affect ray interaction at the surface in a combined form as follows

$$\sigma_{\text{optical}} = (4\sigma^2{}_{\text{slope}} + \sigma^2{}_{\text{specularity}})^{1/2} \qquad (13)$$

Where $\sigma_{\text{optical}}$ is the comprehensive factor, $\sigma_{\text{slope}}$ means the surface slope error, and $\sigma_{\text{specularity}}$ represents the surface specularity error.

*2.5 Evaluation of model parameters*

The variables and constants used in this model are listed in Table 2 with specific

meanings. The geometric parameters were obtained based on the real dimensions of the reactor and the kinetics parameters by fitting the experimental data. Since the reaction rate constant is not known in advance, should it be assumed at first. The $CH_3OH$ production can be numerically calculated and then compared with the experimental data. If the error is not within the allowed value, should the reaction rate constant as aforementioned above be reassumed for expecting results. The mass transfer parameters were estimated by Eqs.(7-9) with the initials referring to the experiment, and the sun position parameters by Eqs.(10) and (11) with the optical variables determined by Eqs.(12) and (13).

*2.6 Validation of numerical results*

Adopting the reaction engineering and diluted species transport modules, Eqs.(2-3) and (4-9) can be solved respectively by the commercial software COMSOL. Besides, the reaction rate can be iterated as the light intensity was taken into account by setting global variables.

The initial conditions with pure $CO_2$ are simulated as shown in Figs. 2 and 3. As observed, the $H_2$ concentration increases sharply at the beginning since the $H^+$ generated by water decomposition penetrates directly through the ion exchange membrane to form $H_2$. Meanwhile, the $O_2$ concentration in the water splitting reactor also rises with a half production of $H_2$. However as the $O_2$ increases stably, the $H_2$ in the $CO_2$ reduction reactor no longer increases and keeps at the rate of nearly

0.85μmol/g, showing that $H_2$ already reaches a balance since it generated by water splitting transforms directly into the $CH_3OH$ and other organic compounds. So at the beginning five hours, even the increasing rate declines gradually, the $CH_3OH$ rises conspicuously with an average speed of 0.8 μmol/g/h, while it then keeps almost no change with the ultimate concentration of 4μmol/g as shown in Fig. 3. Besides, Fig. 3 shows that the average error between the simulation and experimental results is about 13.12%, which is quite small. Moreover, Fig. 4 shows the concentration of methyl formate ($HCOOCH_3$) and acetaldehyde ($CH_3CHO$) as the two by-products during the reaction process, which reaches 1.5μmol/g and 0.4 μmol/g with the average rate of 0.1875 μmol/g/h and 0.05 μmol/g/h respectively within the 8 hours. The $CO_2$ and CO composite process is also numerically calculated with the initial partial pressure of CO set in accordance with the mixing ratio of 1:10 and 1:5 respectively as shown in Figs. 5 and 6, which clearly present that the final $CH_3OH$ concentrations are 7.8 μmol/g and 7.4μmol/g after 8 hours with the relative errors between the simulating and experimental results of 4.41% and 2.92% respectively.

The comparisons show that the numerical and experimental results agree well with each other, so the modelling approach is reliable and accurate enough to predict the photocatalytic $CO_2$ reduction performances in the twin reactor system. Since the photocatalytic $CO_2$ reduction gradually recedes with an ultimately constant $CH_3OH$ concentration, the working conditions of the twin reactor system can be optimized by

means of numerical simulations.

## 3. Results and discussion

### *3.1 Effects of gas mixture ratio*

Pure CO as the reactant gas is specifically simulated so as to unveil its characteristics during the overall process at the ambient pressure and temperature of 1atm and 293K respectively. Fig. 7 shows that the $H_2$ presents almost twice the concentration of $O_2$, while the $CH_3OH$ concentration displays nearly zero due to the non-conversion from hydrogen, which clearly shows the unavailable direct chemical reaction between the pure CO and hydrogen or hydrogen ions. However, very small amount of $CH_3OH$ (less than 0.1μmol/g) exists inevitably due to the following reaction in the reduction reactor:

$$H_2O+CO \xrightarrow{UV,photocatalyst} H_2+CO_2$$
$$CO_2+6H^+ +6e^- \xrightarrow{UV,photocatalyst} CH_3OH+H_2O$$

The overall process at various gas mixture ratios of CO to $CO_2$ was numerically simulated during the whole 20 hours with the carbon elements symbolized as $C_x$ from $CO_2$ and $C_y$ from CO for easy analysis of the carbon trails existing in methanol. Fig.8 displays the processing amount of $C_xH_3OH$ as well as $C_yH_3OH$ at the CO to $CO_2$ ratio of 1:10. During the first 8 hours, it can be observed that the $C_xH_3OH$ has a higher production rate of 0.53 μmol/g/h, while only 0.45 μmol/g/h for the $C_yH_3OH$. After then, it changes little for the concentration of $C_xH_3OH$ with a stable amount of 4.2μmol/g at the 20th hour. But for $C_yH_3OH$, the concentration always increases and

eventually reaches about 4.6 μmol /g after 20 hours. It shows that the CO can easily transform into the methanol and other organic compounds through the chemical chains as aforementioned above compared with $CO_2$. As shown in Fig. 9, the production of $C_xH_3OH$ declines with the CO to $CO_2$ ratio of 1:5 compared with the case of 1:10, and only arrives at 3.6μmol/g for the maximum concentration. As for $C_yH_3OH$, the concentration reaches the peak of nearly 3.75 μmol/g at the time of 7.5h, then it decreases to 2.1 μmol /g after 20 hours and finally presents a declining tendency. Since CO plays a double role during the $CH_3OH$ production, may the $CH_3OH$ increase due to its positive effect with a small amount, while should other organic compounds unexpectedly emerge with an excessive CO ratio. Fig. 10 shows the $CH_3CHO$ concentration at various gas mixture ratios, which clearly presents the always small value less than 0.5 μmol/g at the first 5 hours. But the $CH_3CHO$ production rate increases as the chemical process continues, and it presents a higher value at a more intensive CO concentration. Besides, as the ratio of CO to $CO_2$ changes from 1/20 to 1/2, the $CH_3CHO$ concentration increases from 1.5 μmol/g to 3.75 μmol/g after 20 hours.

Figs.8-10 fully explain the mechanisms of the CO dominance in the photocatalytic process, which can be described by the following three reactions.

$$(1)\quad CH_3OH+CO \xrightarrow{UV,photocatalyst} HCOOCH_3$$

$$(2)\quad HCOOCH_3+CO \xrightarrow{UV,photocatalyst} CH_3CHO+CO_2$$

$$(3)\quad HCOOCH_3+4H^+ +4e^- \xrightarrow{UV,photocatalyst} 2CH_3OH$$

When a small amount of CO gas exists in the reactor, the CO reacts with $CH_3OH$ to form $HCOOCH_3$ as reaction (1). Due to the excessive $H_2$, the $HCOOCH_3$ reacts with $H_2$ and then generates $CH_3OH$ as reaction (3). In this case, the CO promotes $CH_3OH$ production. However, if CO gas is excessive, the CO will react with $CH_3OH$ to form $HCOOCH_3$ at first, then the remaining CO continues to react with $HCOOCH_3$ to produce $CH_3CHO$ as reaction (2), which prevents $HCOOCH_3$ from reacting with $H_2$, resulting in an indirect consumption of $CH_3OH$.

The aforementioned conclusion about the gas mixture ratio can be of benefit to the design and application of photocatalytic reactor systems. For the twin reactor, the optimal CO to $CO_2$ ratio as well as reaction time can be recommended with reference to the light intensity distribution and reactor structure. Moreover, increasing the byproduct of $CH_3CHO$ during the photocatalytic process proves efficient to prevent the side effect as reaction (2).

*3.2 Effects of pressure*

The mixture pressure in the reactor is of great importance for photocatalytic reactions. According to Henry's law, the partial pressure of the mixture above the liquid surface can directly affect the gas solubility. Besides, the mass transfer rate between the gas and liquid is related greatly with the partial pressure in terms of the two-film theory. Fig. 11 presents the production of $CH_3OH$ at various pressures during the 20 hours. It can be seen that as the initial pressure in the reactor goes up,

346 the $CH_3OH$ yield increases. When the initial pressure reaches 20atm, the $CH_3OH$
347 concentration arrives at 14.5 μmol/g at 20 hours, which is 52.6% higher than that of
348 9.5 μmol/g at the initial pressure of 1atm. As for the efficiency, increasing the initial
349 pressure in the reactor will consume more energy, so a viable operating pressure
350 should be determined for the photocatalytic reactor in potential engineering
351 applications.

352 *3.3 Effects of temperature*

353 The Henry constant can well represent the solubility of $CO_2$ and CO in the
354 electrolyte. As observed from Table 3, the Henry constant increases as the temperature
355 rises. Besides, the diffusion coefficients of the gas-gas as well as gas-liquid depend
356 also upon the temperature according to Eq.(9), so the mass transfer correlates strongly
357 with the temperature. Fig.12 shows the $CH_3OH$ concentration change at various
358 temperatures, from which can be seen that the $CH_3OH$ concentration increases with
359 increasing the temperature, resulting from the comprehensive effects of the solubility
360 and mass transfer rate. At the temperature of 273K, the ultimate $CH_3OH$ concentration
361 at the 20th hour is 6 μmol/g, while at 333K it approaches 11μmol/g, presenting an
362 increase of 83.2%, which shows that the conversion efficiency can be greatly
363 improved by increasing the temperature.

364 *3.4 Effects of light intensity*

365 Based on the optical parameters of the physical model aforementioned, the sun

366 light model is developed and the two dimensional distribution of light intensity on a
367 cross-section of the reactor is achieved by adopting the software SOLTRACE. Fig. 13
368 shows transient solar flux distribution in the reactor at 8:00, 12:00 and 16:00
369 respectively, in which the positive direction of the X-axis stands for the west of the
370 reactor and the positive direction of the Y-axis represents the zenith of the twin reactor.
371 The distribution of light intensity at 8:00 is shown in Fig.13(a), which presents a
372 non-uniform light intensity scattering in the reactor with 832W/m$^2$ on the east side
373 while only 205W/m$^2$ on the west side, and the average light intensity is about
374 331W/m$^2$. As observed from Fig. 13(b), the reactor receives the sunlight vertically at
375 12:00, so the light intensity arrives at the maximum value in the center while
376 minimum value at both sides, due to the combined effects of the reflection and
377 refraction by the glass container and colored solution with the iron ion. The average
378 light intensity can reach nearly 620W/m$^2$ in the reactor. Fig. 13(c) presents the
379 irradiation at 16:00 from the west side of the reactor with the average light intensity of
380 330W/m$^2$.

381 From 8:00 to 16:00, the average light intensity is obtained and shown in Fig.14,
382 which is fitted to the following equation:

383 $$I=-1996+435Hr-18Hr^2 \quad (14)$$

384 It can be seen from Fig.14 that the results from the fitting curve agree well with the
385 simulated data, so the fitting equation is reliable enough to predict the average light

intensity change over time. Together with the chemical reaction engineering module, the photocatalytic $CO_2$ reduction combined with the water splitting process can be numerically simulated within the 8 hours (8:00-16:00) at the temperature of 293K and pressure of 1atm. Fig.15 shows the concentration changes of $O_2$, $H_2$ and $CH_3OH$ over time, proving that the $CH_3OH$ product using the sun light source is less than that using the artificial light source in the experiment of Cheng et al.[25]. As also clearly presented, the $CH_3OH$ concentration reaches the climax of 4.6 μmol/g about 3.5 hours later (11:30), and then it begins to decrease gradually due to the weakened light intensity. Fig. 16 shows the reaction rates of the photocatalytic $CO_2$ reduction and water splitting process. It can be seen that as the light intensity decreases, the photocatalytic water splitting reaction becomes slow, resulting in the reduced $H_2$ for $CO_2$ reduction. The $CH_3OH$ generating rate is lower than the consuming rate of side reaction, leading to a reduced $CH_3OH$ concentration.

Since the experimental study with the artificially unchanged light intensity could not totally represent the photocatalytic $CO_2$ reduction mechanism, the numerical method with the natural sunlight changing over time demonstrates an attractive superiority, which is closer to the real chemical process.

## 4. Conclusions

The photocatalytic reduction of $CO_2$ by CO co-feed combined with photocatalytic water splitting in a novel twin reactor was modeled and numerically investigated.

The $CH_3OH$ concentration almost linearly increases with increasing the gas mixture ratio of CO to $CO_2$, due to the direct conversion from CO to $CH_3OH$. However, the excessive CO will react with $HCOOCH_3$ to form $CH_3CHO$ unexpectedly, resulting in a reduced $CH_3OH$ concentration. Besides, with the temperature and pressure increase, the $CH_3OH$ production rises owing to the enhanced mass transfer.

The numerical method with the natural sunlight in this work proves a more accurate photocatalytic $CO_2$ reduction process compared with the experiment, and the yield of $CH_3OH$ is reduced due to the changing light intensity. It suggests the artificial light intensity adjusted with time in the photocatalytic experiment, so as to obtain a more reliable result.

**Acknowledgment**

The financial support for this research from the National Natural Science Foundation of China (Grant No. 50776032) is gratefully acknowledged. The authors also thank the support provided by the Royal Society International Project of UK (IE150489).

## References


[1] Baran T, Wojtyła S, Dibenedetto A, Aresta M, Macyk W. Zinc sulfide functionalized with ruthenium nanoparticles for photocatalytic reduction of $CO_2$. Applied Catalysis B: Environmental 2015;178:170-6.

[2] Huang Q, Yu J, Cao S, Cui C, Cheng B. Efficient photocatalytic reduction of $CO_2$ by amine-functionalized g-$C_3N_4$. Appl Surf Sci 2015;358:350-5.

[3] Tahir B, Tahir M, Amin NS. Gold–indium modified $TiO_2$ nanocatalysts for photocatalytic $CO_2$ reduction with $H_2$ as reductant in a monolith photoreactor. Appl Surf Sci 2015;338:1-14.

[4] Yuan K, Yang L, Du X, Yang Y. Performance analysis of photocatalytic $CO_2$ reduction in optical fiber monolith reactor with multiple inverse lights. Energ Convers Manage 2014;81:98-105.

[5] Yuan K, Yang L, Du X, Yang Y. Numerical analysis of photocatalytic $CO_2$ reduction in optical fiber monolith reactor with optimized structures. Energ Convers Manage 2014;87:258-66.

[6] Tahir M, Amin NS. Recycling of carbon dioxide to renewable fuels by photocatalysis: Prospects and challenges. Renewable and Sustainable Energy Reviews 2013;25:560-79.

[7] Chiu FP, Kuo HI, Chen CC, Hsu CS. The energy price equivalence of carbon taxes and emissions trading—Theory and evidence. Appl Energ 2015;160:164-71.

[8] Liu Y, Zhou Y, Wu W. Assessing the impact of population, income and technology on energy consumption and industrial pollutant emissions in China. Appl Energ 2015;155:904-17.

[9] Wang Q, Su B, Sun J, Zhou P, Zhou D. Measurement and decomposition of energy-saving and emissions reduction performance in Chinese cities. Appl Energ 2015;151:85-92.

[10] Sim LC, Leong KH, Saravanan P, Ibrahim S. Rapid thermal reduced graphene oxide/Pt-$TiO_2$ nanotube arrays for enhanced visible-light-driven photocatalytic reduction of $CO_2$. Appl Surf Sci 2015.

[11] Tahir M, Amin NS. Photocatalytic $CO_2$ reduction with $H_2$ as reductant over copper and indium co-doped $TiO_2$ nanocatalysts in a monolith photoreactor. Applied Catalysis A: General 2015;493:90-102.

[12] Inoue T, Fujishima A, Satoshi K, Honda K. Photoelectrocatalytic reduction of carbon dioxide in aqueous suspensions of semiconductor powders. Nature 1979;277:637-8.

[13] Tahir M, Amin NS. Advances in visible light responsive titanium oxide-based photocatalysts for $CO_2$ conversion to hydrocarbon fuels. Energ Convers Manage 2013;76:194-214.

[14] Broberg Viklund S, Johansson MT. Technologies for utilization of industrial excess heat: Potentials for energy recovery and $CO_2$ emission reduction. Energ Convers Manage 2014;77:369-79.

[15] Jain S, Vardia J, Ameta R, Ameta SC. Use of malachite green as photocatalyst in reduction of sodium and potassium carbonates. Energ Convers Manage 2004;45:1233-42.

[16] Tahir B, Tahir M, Amin NS. Performance analysis of monolith photoreactor for $CO_2$ reduction with $H_2$. Energ Convers Manage 2015;90:272-81.

[17] Wang T, Yang L, Du X, Yang Y. Numerical investigation on $CO_2$ photocatalytic reduction in optical fiber monolith reactor. Energ Convers Manage 2013;65:299-307.

[18] Ola O, Maroto-Valer MM. Transition metal oxide based $TiO_2$ nanoparticles for visible light induced $CO_2$ photoreduction. Applied Catalysis A: General 2015;502:114-21.

[19] Ola O, Maroto-Valer MM. Review of material design and reactor engineering on $TiO_2$

462 photocatalysis for $CO_2$ reduction. Journal of Photochemistry and Photobiology C: Photochemistry
463 Reviews 2015;24:16-42.
464 [20] Nong G, Chen Y, Li M, Zhou Z. Generation of hydrogen free radicals from water for fuels by
465 electric field induction. Energ Convers Manage 2015;105:545-51.
466 [21] Waskasi MM, Hashemianzadeh SM, Mostajabi Sarhangi O, Harzandi AP. Computational model
467 of hydrogen production by Coumarin-dye-sensitized water splitting to absorb the visible light in a local
468 electric field. Energ Convers Manage 2012;62:154-64.
469 [22] Thampi KR, Kiwi J, Gratzel M. Methanation and photo-methanation of carbon dioxide at room
470 temperature and atmospheric pressure. Nature 1987;327:506-8.
471 [23] Lo CC, Hung CH, Yuan CS, Wu JF. Photoreduction of carbon dioxide with $H_2$ and $H_2O$ over
472 $TiO_2$ and $ZrO_2$ in a circulated photocatalytic reactor. Sol Energ Mat Sol C 2007;91:1765-74.
473 [24] Shinichi I, Ryota D. Hydrogen production from water and conversion of carbon dioxide to
474 useful chemicals by room temperature photoelectrocatalysis. Catal Today 1996;27:271-7.
475 [25] Cheng YH, Nguyen VH, Chan HY, Wu JCS, Wang WH. Photo-enhanced hydrogenation of $CO_2$
476 to mimic photosynthesis by CO co-feed in a novel twin reactor. Appl Energ 2015;147:318-24.
477 [26] Lee WH, Liao CH, Tsai MF, Huang CW, Wu JCS. A novel twin reactor for $CO_2$ photoreduction
478 to mimic artificial photosynthesis. Applied Catalysis B: Environmental 2013;132-133:445-51.
479 [27] Yu SC, Huang CW, Liao CH, Wu JCS, Chang ST, Chen KH. A novel membrane reactor for
480 separating hydrogen and oxygen in photocatalytic water splitting. J Membrane Sci 2011;382:291-9.
481 [28] Lin H, Valsaraj K. An optical fiber monolith reactor for photocatalytic wastewater treatment.
482 Aiche J 2006:2271-80.
483 [29] Herrmann JM. Heterogeneous photocatalysis: an emerging discipline involving multiphase
484 systems. Catal Today 1995;24:157-64.
485 [30] Denny F, Scott J, Peng GD, Amal R. Channelled optical fibre photoreactor for improved air
486 quality control. Chem Eng Sci 2010;65:882-9.
487 [31] Ueyama K, Hatanaka J. Salt effect on solubility of nonelectrolyte gases and liquids. Chem Eng
488 Sci 1982;37:790–2.
489 [32] Ryszard P, Wadysaw M. Kinetics of Reaction Between Carbon-Dioxide and Hydroxyl Ions in
490 Aqueous-Electrolyte Solutions. Chem Eng Sci 1988;43:1677-84.
491 [33] Rathore M, Kapuno R. Engineering heat transfer: Jones & Bartlett; 2011.
492 [34] Spencer GH, Murty M. General Ray-Tracing Procedure. Journal of the Optical Society of
493 America 1962;52:672-8.

**Table 1**

Changes of enthalpy and Gibbs free energy in the $CO_2$ photoreduction reactions[25].

| Reactions | $\Delta H^0$ (kJ/mol) | $\Delta G^0$ (kJ/mol) |
|---|---|---|
| (1) $CO_2(g)+3H_2(g)\rightarrow CH_3OH(l)+H_2O(l)$ | −137.8 | −10.7 |
| (2) $CO(g)+CH_3OH(l)\rightarrow HCOOCH_3(l)$ | −25.6 | 6.6 |
| (3) $CO_2(g)+H_2(g)+CH_3OH(l)\rightarrow HCOOCH_3(l)+H_2O(l)$ | −31.8 | 25.8 |
| (4) $HCOOCH_3(l)+2H_2(g)\rightarrow 2CH_3OH(l)$ | −99.7 | −35.1 |
| (5) $HCOOCH_3(l)+CO(g)\rightarrow CH_3CHO(l)+CO_2(g)$ | −96.5 | −86.7 |

**Table 2**

Model parameters for photocatalytic $CO_2$ reduction by CO co-feed.

| Type | Variables | Values | Unit |
|---|---|---|---|
| kinetics | $k_1$ | 3.3E-9 | $m^3/(s \cdot mol)$ |
| | $k_2$ | 1.7E-2 | $m^9/(s \cdot mol^3)$ |
| | $k_3$ | 2.3E-4 | $m^3/(s \cdot mol)$ |
| | $k_4$ | 1.7E-4 | $m^3/(s \cdot mol)$ |
| | $k_5$ | 5.8E-6 | $m^6/(s \cdot mol^2)$ |
| | $k_6$ | 8.1E-3 | $m^3/(s \cdot mol)$ |
| Geometry | $L$ | 11.46 | cm |
| | $R_1$ | 5 | cm |
| | $R_2$ | 4 | cm |
| Mass transfer | $D_L$ | 1.9809E-9 | $m^2/s$ |
| | $D_G$ | 1.41E-7 | $m^2/s$ |
| | $\delta_G$ | 0.1 | mm |
| | $\delta_L$ | 0.1 | mm |
| | $h_{H^+}$ | 0 | |
| | $h_{Fe^{2+}}$ | 0.049 | |
| | $h_{Fe^{3+}}$ | 0.054 | |
| | $h_{SO_4^{2-}}$ | 0.029 | |
| | $h_{Cl^-}$ | 0.021 | |

| | | | |
|---|---|---|---|
| | $h_{CO^2}$ | -0.019 | |
| | $h_{CO}$ | 0.0283 | |
| | $H_{0CO}$ | 5.43E+6 | kPa |
| | $H_{0CO_2}$ | 1.44E+5 | kPa |
| Initial value | $C_{CO_2}$ | 30.73 | $mol/m^3$ |
| | $C_{CO}$ | 0.095 | $mol/m^3$ |
| | $C_{SO_4^{2-}}$ | 1.21 | $mol/m^3$ |
| | $C_{Fe^{2+}}$ | 8.8 | $mol/m^3$ |
| | $C_{Fe^{3+}}$ | 8.8 | $mol/m^3$ |
| | $I$ | 900 | $W/m^2$ |
| | $m$ | 1 | |
| Sun position | *Day* | 200 | |
| | *Hr* | 8-16 | |
| | $L$ | 40°5’ | |
| | *Shape* | Pillbox | |
| Optical property | $Rf_{glass}$ | 0.05 | |
| | $Tr_{glass}$ | 0.95 | |
| | $Ab_{glass}$ | 0 | |
| | $n_{glass}$ | 1.6 | |
| | $Rf_{solution}$ | 0.2 | |

| | |
|---|---|
| $Tr_{solution}$ | 0.48 |
| $Ab_{solution}$ | 0.32 |
| $n_{solution}$ | 1.3 |
| *Slope error(mrad)* | 3.5 |
| *Specularity error(mrad)* | 0.2 |

**Table 3**

Henry constants at various temperatures.

| Gas \ $T$(K) | 273 | 278 | 283 | 288 | 293 | 298 | 303 | 308 | 313 | 318 | 323 | 333 |
|---|---|---|---|---|---|---|---|---|---|---|---|---|
| CO ($H_x$×$10^{-6}$ kPa) | 3.57 | 4.01 | 4.48 | 4.95 | 5.43 | 5.88 | 6.28 | 6.68 | 7.05 | 7.39 | 7.71 | 8.32 |
| $CO_2$($H_x$×$10^{-5}$ kPa) | 0.37 | 0.8 | 1.05 | 1.24 | 1.44 | 1.66 | 1.88 | 2.12 | 2.36 | 2.60 | 2.87 | 3.46 |

$$H_c = \frac{H_x M_{solvent}}{1000\rho}$$

Fig.1. Schematic of photocatalytic $CO_2$ reduction and $H_2O$ splitting in the twin reactor.

Fig.2. $H_2$ and $O_2$ production during photocatalytic reduction of pure $CO_2$ with simultaneous $H_2O$ splitting.

Fig.3. $CH_3OH$ production during photocatalytic reduction of pure $CO_2$ with simultaneous $H_2O$ splitting.

Fig.4. $CH_3CHO$ and $HCOOCH_3$ production during photocatalytic reduction of pure $CO_2$ with simultaneous $H_2O$ splitting.

Fig.5. $CH_3OH$ concentration at the CO to $CO_2$ ratio of 1:10.

Fig.6. $CH_3OH$ concentration at the CO to $CO_2$ ratio of 1:5.

Fig.7. $H_2$, $O_2$ and $CH_3OH$ concentrations with the pure CO as the reactant gas.

Fig.8. Total $CH_3OH$ concentration, $C_xH_3OH$ and $C_yH_3OH$ concentrations at the CO to $CO_2$ ratio of 1:10.

Fig.9. Total $CH_3OH$ concentration, $C_xH_3OH$ and $C_yH_3OH$ concentrations at the CO to $CO_2$ ratio of 1:5.

Fig.10. $CH_3CHO$ concentrations at various CO to $CO_2$ gas mixture ratios.

Fig.11. $CH_3OH$ concentration change with time at various pressures.

Fig.12. $CH_3OH$ concentration change with time at various temperatures.

Fig.13. Light intensity distribution in $CO_2$ reduction reactor. (a) 8:00, (b) 12:00, (c) 16:00.

Fig.14. Average light intensity change over time under the sun light.

Fig.15. Concentration changes of $H_2$, $O_2$ and $CH_3OH$ over time under the sun light.

Fig.16. Reaction rate changes of water splitting and $CO_2$ reduction over time under the sun light.

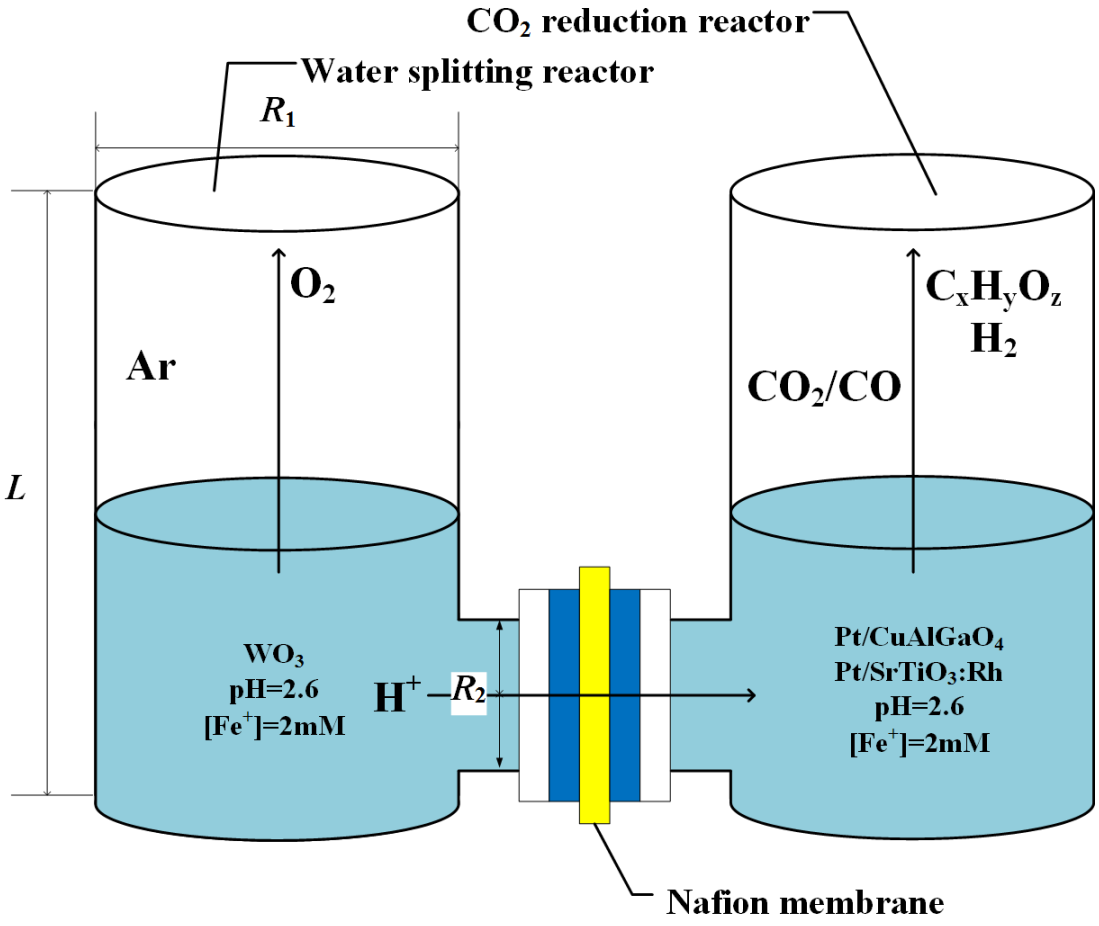
CO2 reduction reactor
Water splitting reactor
R1
O2
Ar
L
CxHyOz
H2
CO2/CO
WO3
pH=2.6
[Fe+]=2mM
H+
R2
Pt/CuAlGaO4
Pt/SrTiO3:Rh
pH=2.6
[Fe+]=2mM
Nafion membrane

Fig.1.

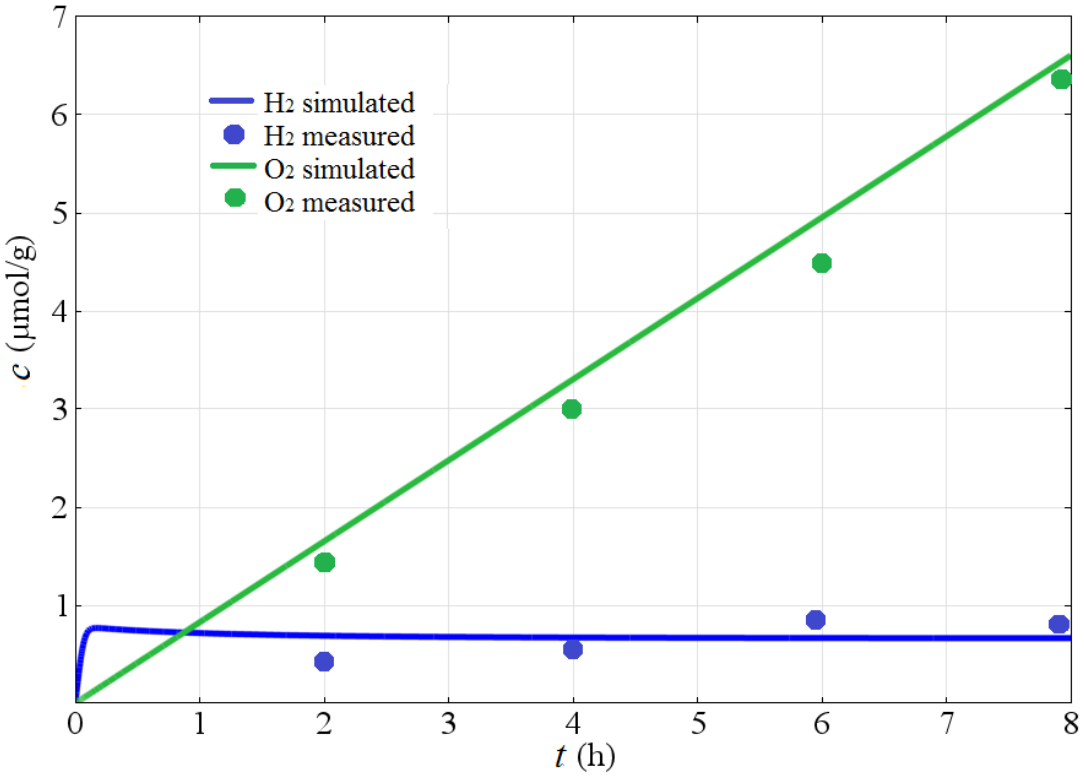
H2 simulated
H2 measured
O2 simulated
O2 measured
c (μmol/g)
t (h)
0
1
2
3
4
5
6
7
8

Fig.2.

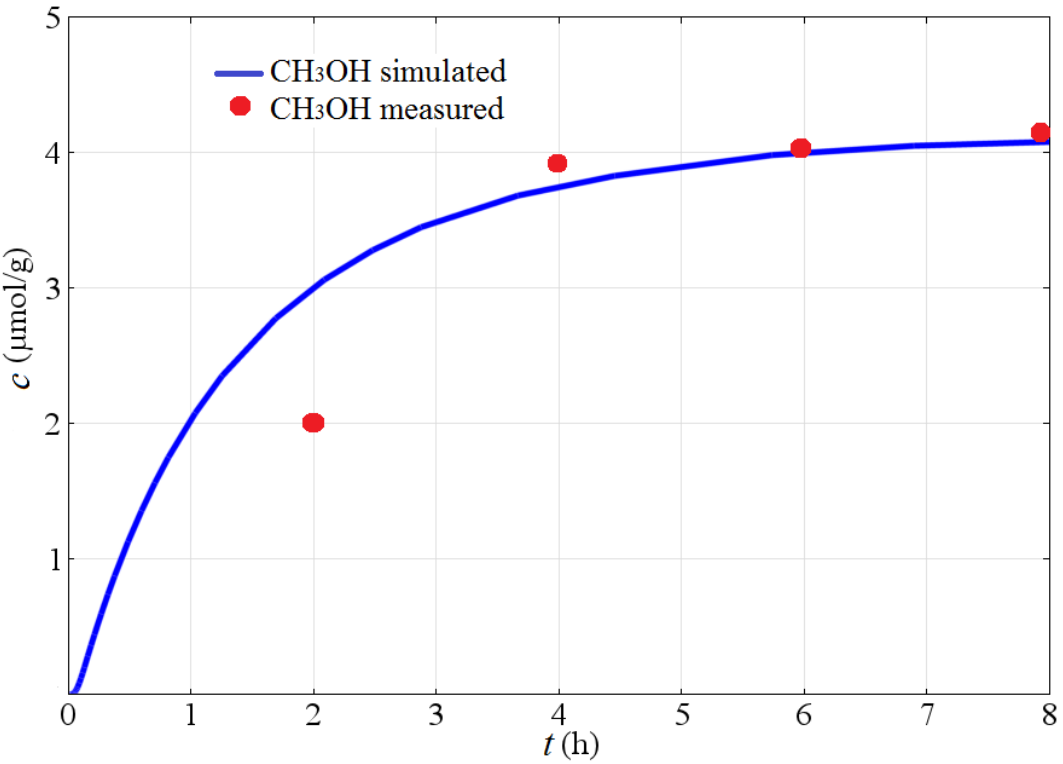


Fig.3.

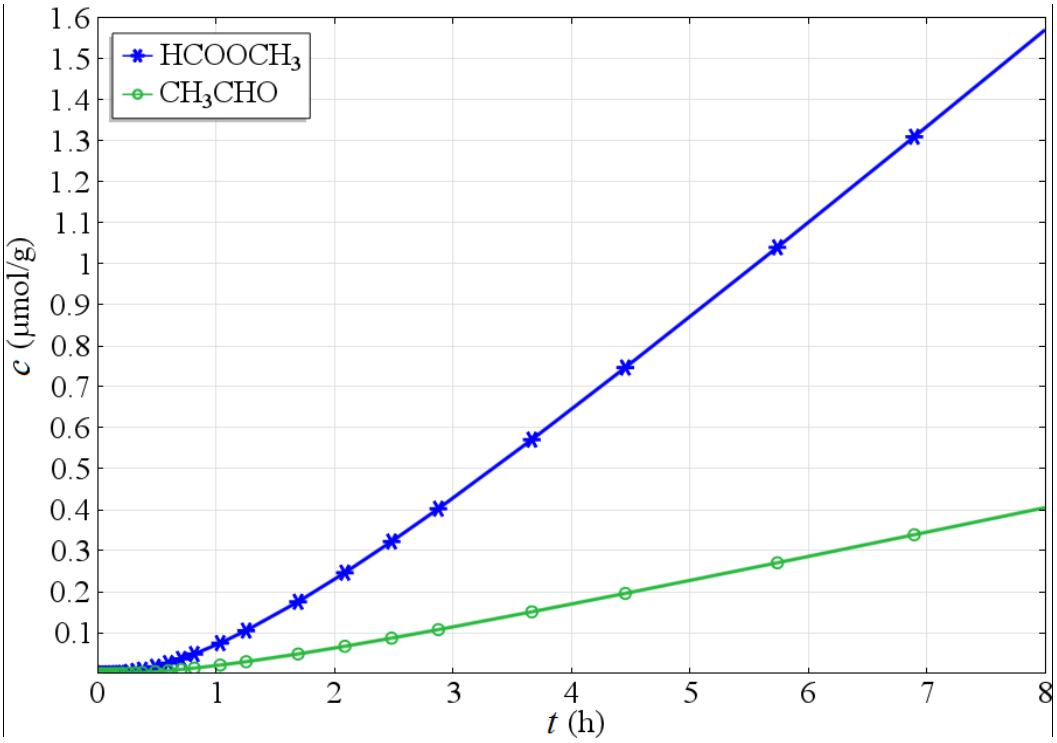
HCOOCH3
CH3CHO
c (μmol/g)
t (h)
1.6
1.5
1.4
1.3
1.2
1.1
1
0.9
0.8
0.7
0.6
0.5
0.4
0.3
0.2
0.1
0
1
2
3
4
5
6
7
8

Fig.4.

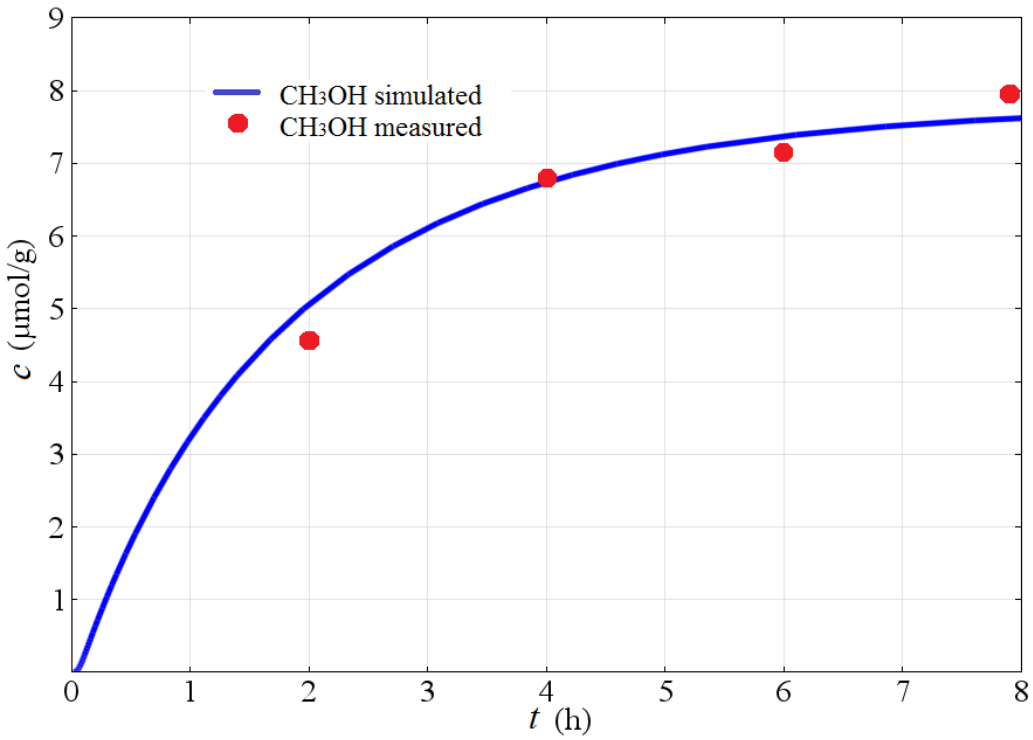


Fig.5.

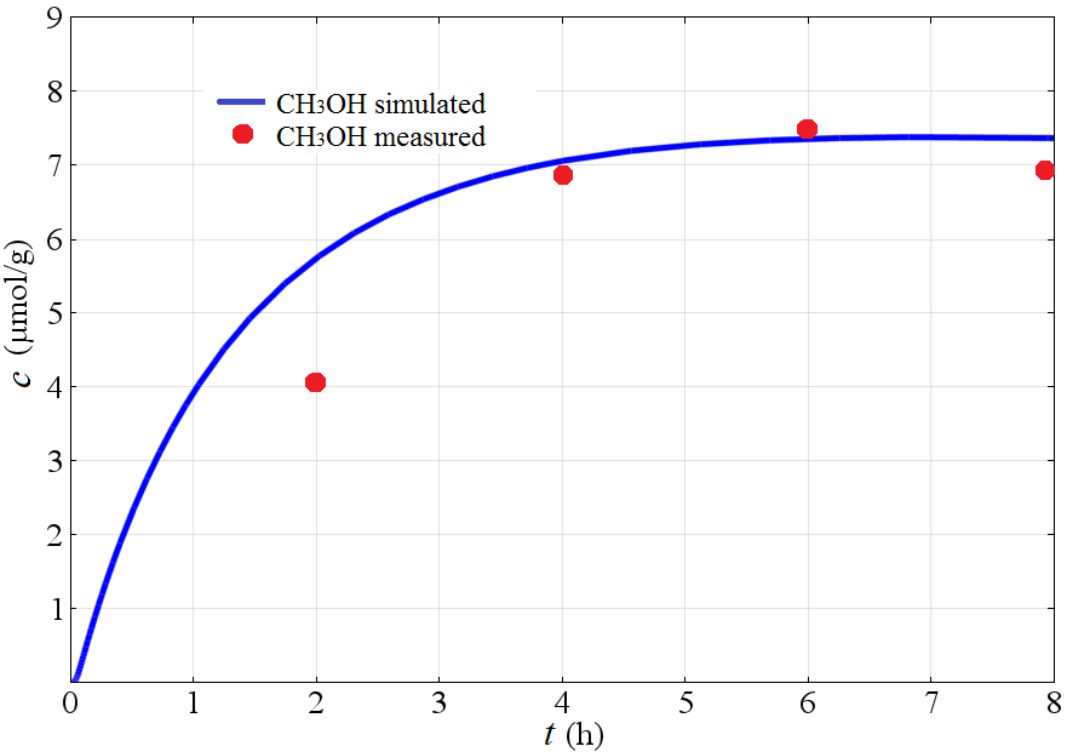


Fig.6.

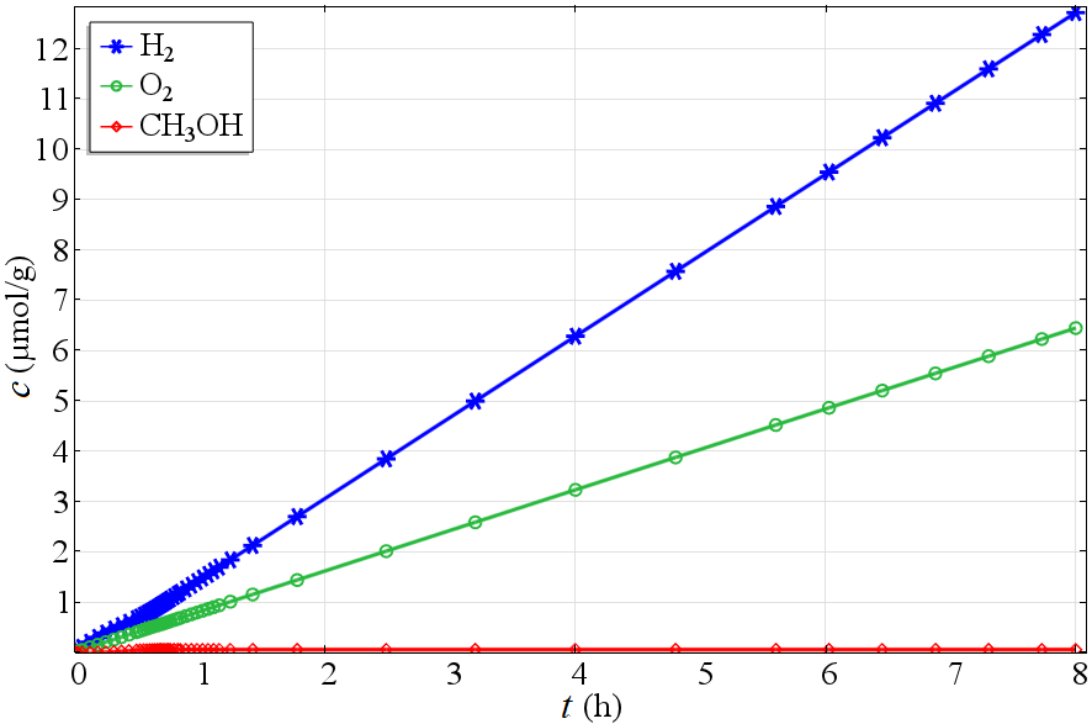


Fig.7.

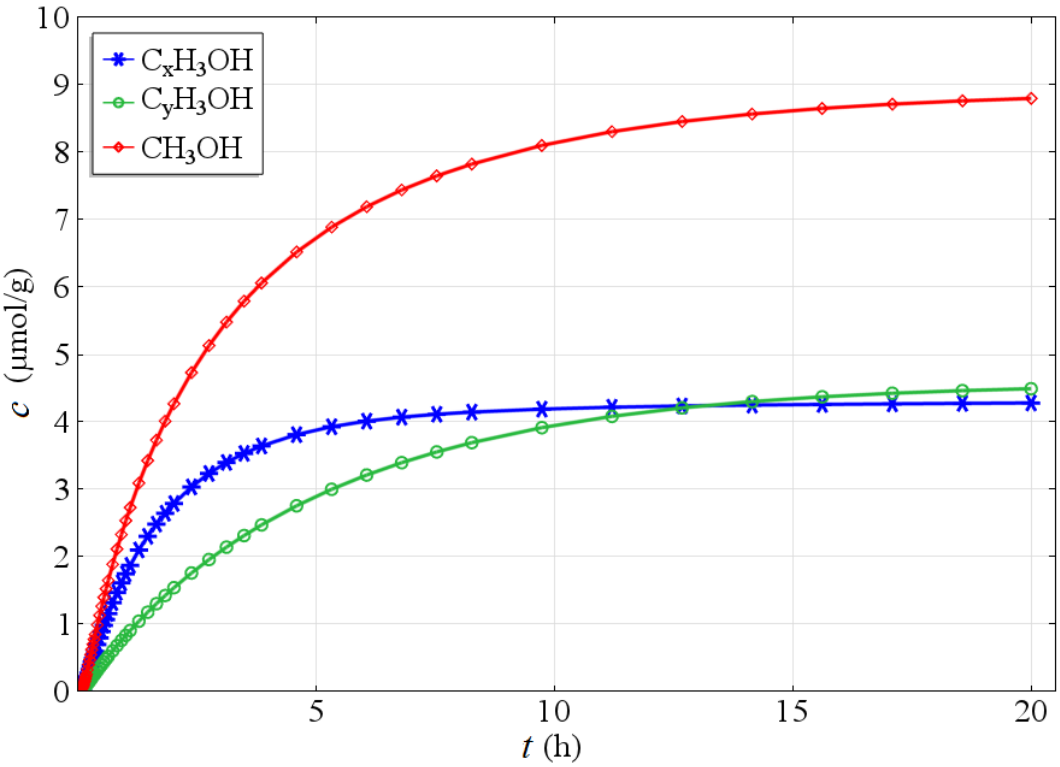


Fig.8.

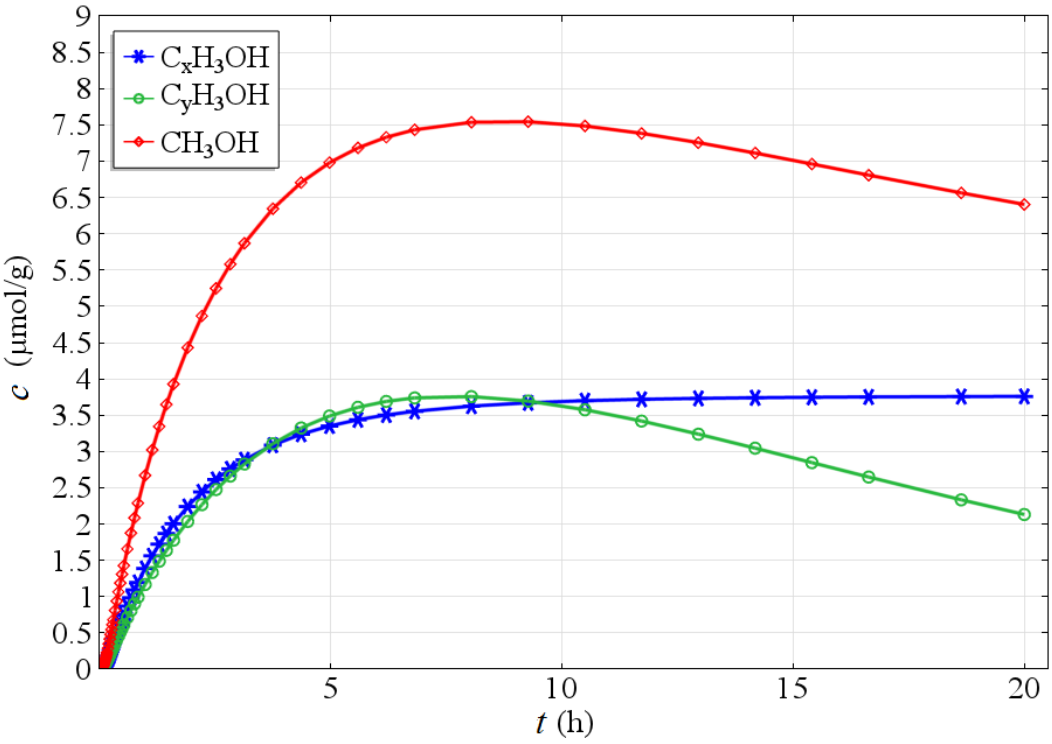
$C_xH_3OH$
$C_yH_3OH$
$CH_3OH$
c (μmol/g)
t (h)
0
0.5
1
1.5
2
2.5
3
3.5
4
4.5
5
5.5
6
6.5
7
7.5
8
8.5
9
5
10
15
20

Fig.9.

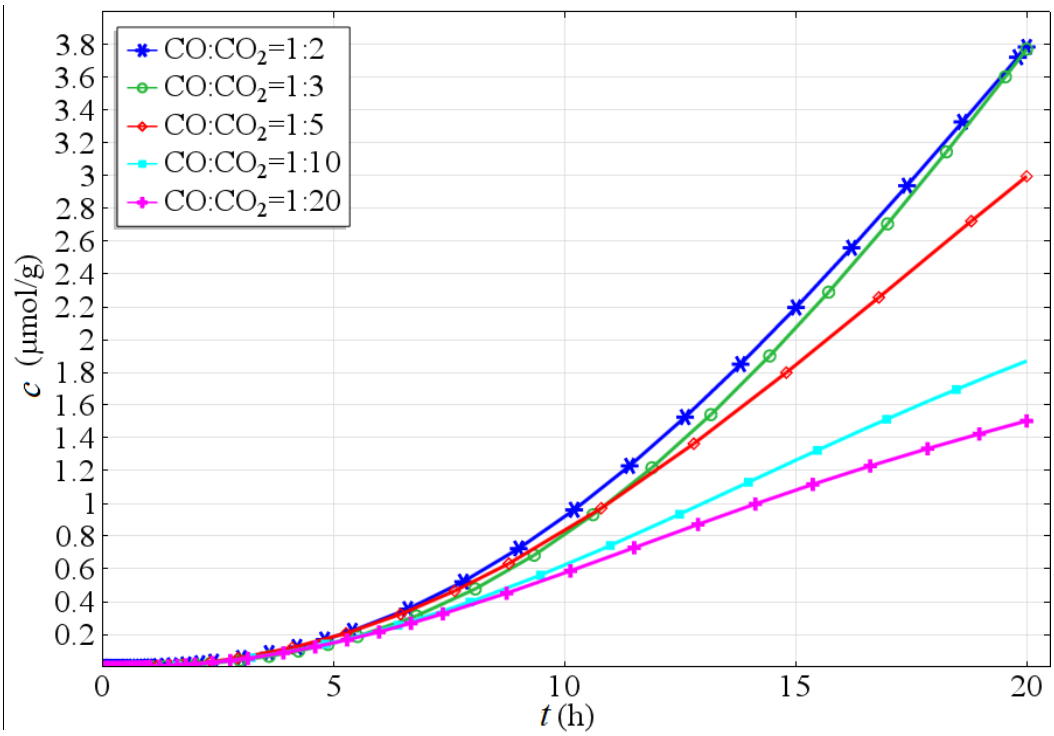
CO:CO2=1:2
CO:CO2=1:3
CO:CO2=1:5
CO:CO2=1:10
CO:CO2=1:20
c (μmol/g)
t (h)
0
5
10
15
20
0.2
0.4
0.6
0.8
1
1.2
1.4
1.6
1.8
2
2.2
2.4
2.6
2.8
3
3.2
3.4
3.6
3.8

Fig.10.

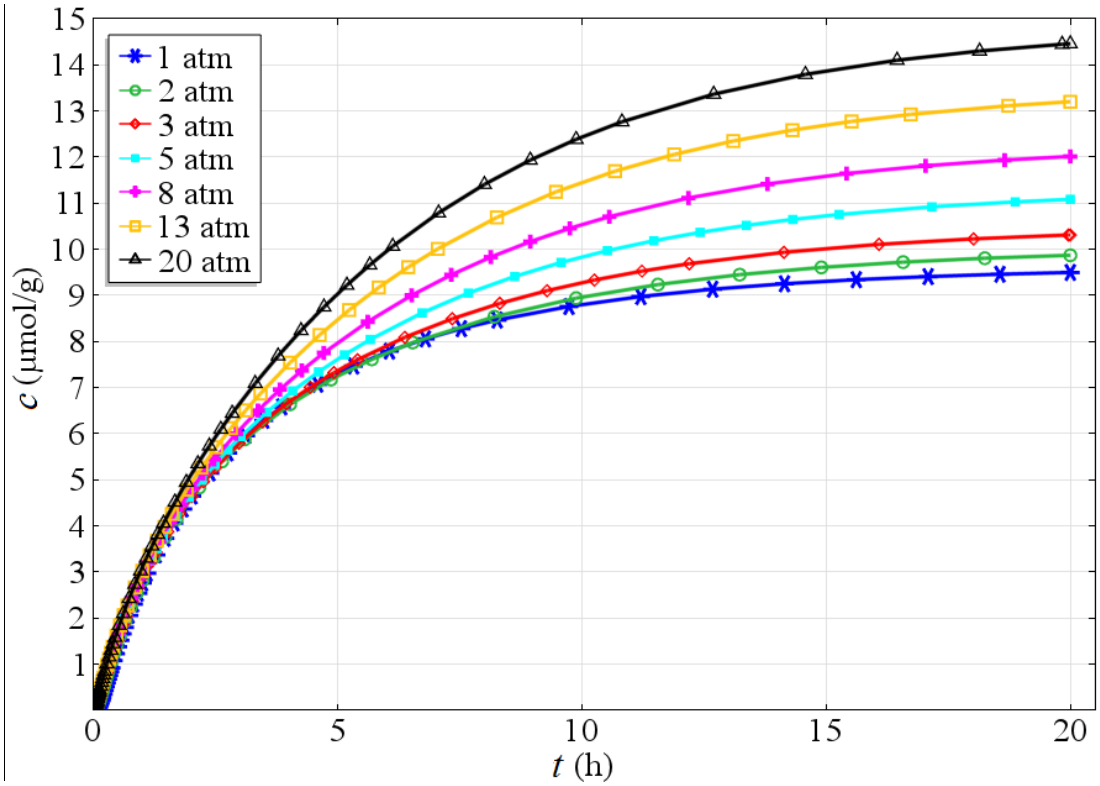
1 atm
2 atm
3 atm
5 atm
8 atm
13 atm
20 atm
c (μmol/g)
t (h)
0
5
10
15
20
1
2
3
4
5
6
7
8
9
10
11
12
13
14
15

Fig.11.

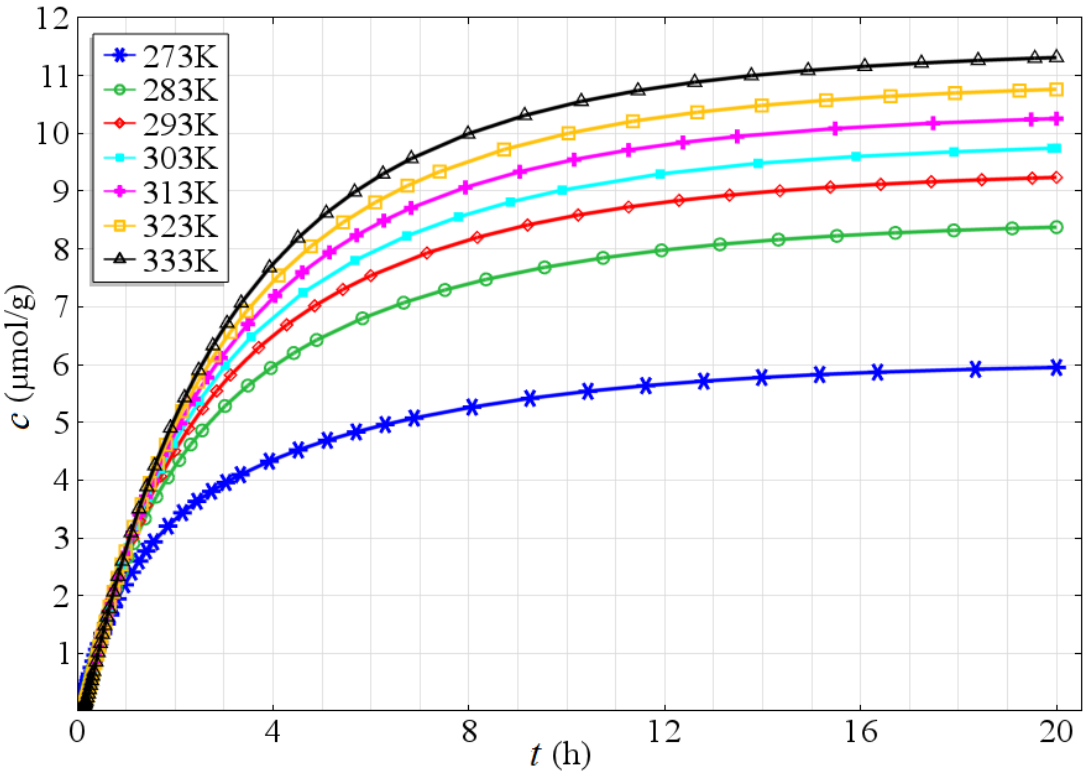
273K
283K
293K
303K
313K
323K
333K
c (μmol/g)
t (h)
0
4
8
12
16
20
1
2
3
4
5
6
7
8
9
10
11
12

Fig.12.

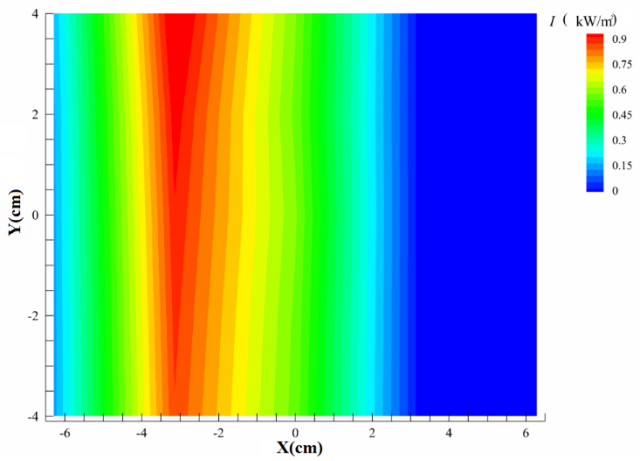
I ( kW/m²)
0.9
0.75
0.6
0.45
0.3
0.15
0
Y(cm)
X(cm)

(a)

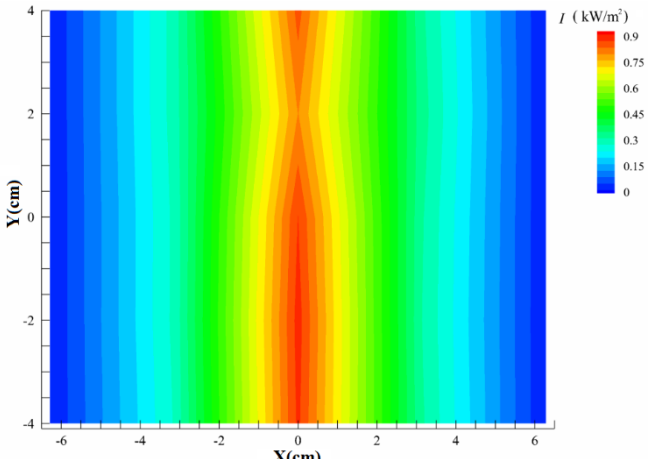
I ( kW/m²)
0.9
0.75
0.6
0.45
0.3
0.15
0
Y(cm)

(b)

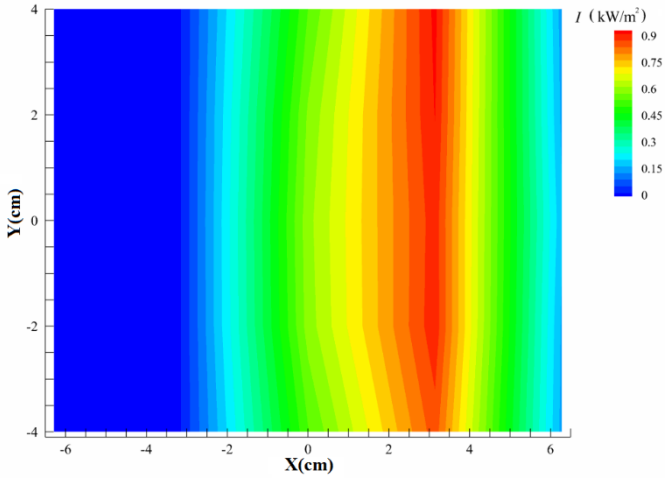
I ( kW/m²)
0.9
0.75
0.6
0.45
0.3
0.15
0
Y(cm)
X(cm)

(c)

Fig.13.

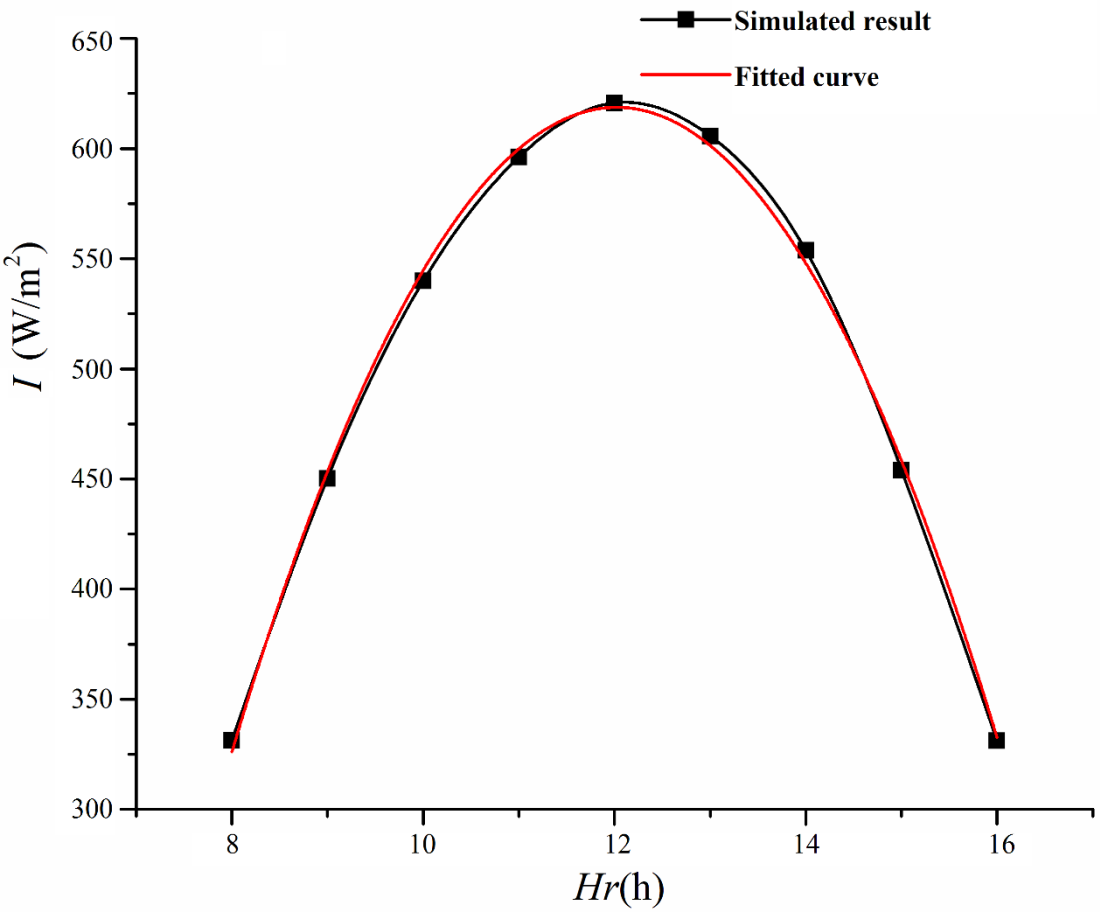
Simulated result
Fitted curve
650
600
550
500
450
400
350
300
I (W/m2)
8
10
12
14
16
Hr(h)

Fig.14.

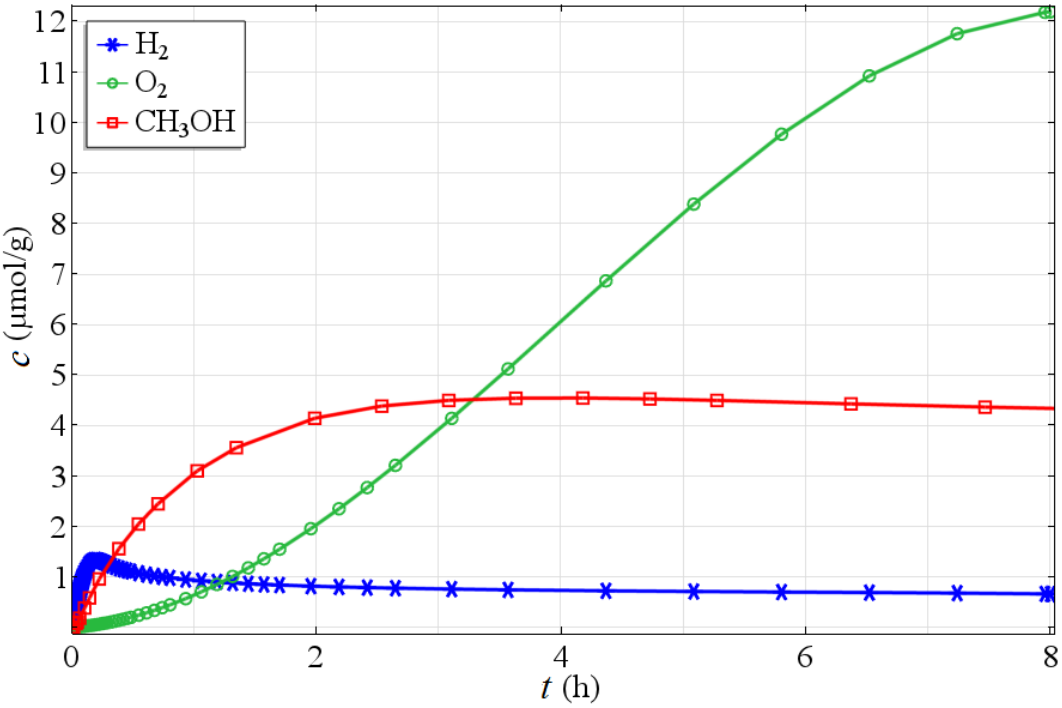


Fig.15.

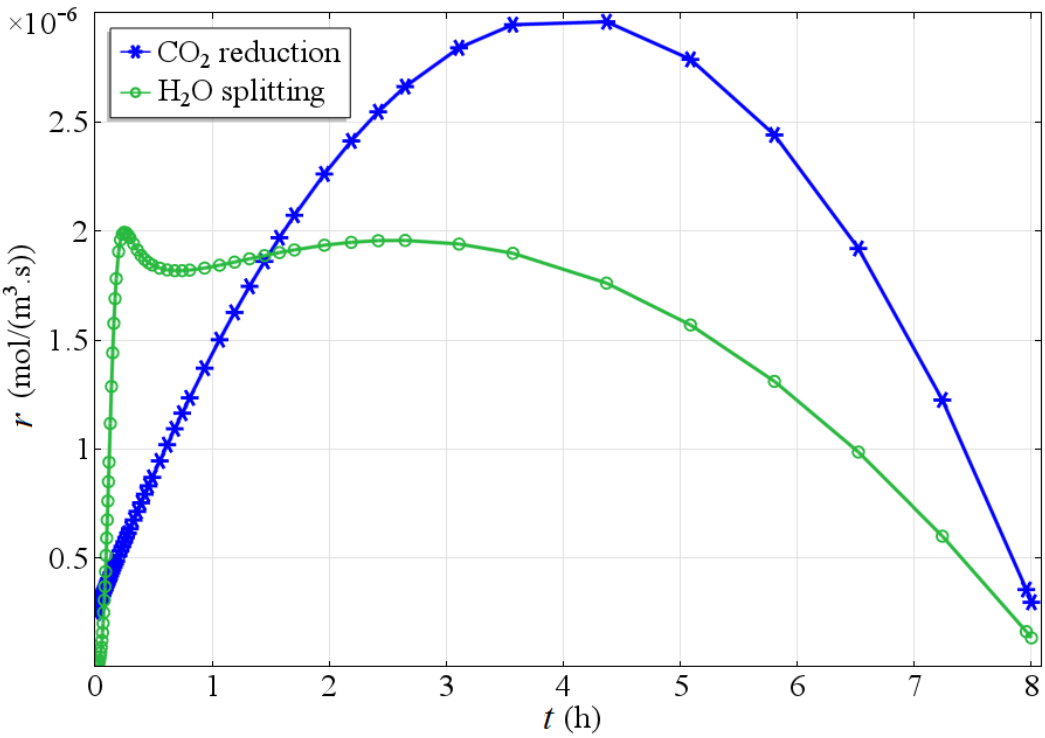
×10^-6
CO2 reduction
H2O splitting
r (mol/(m^3.s))
t (h)
0
0.5
1
1.5
2
2.5
0
1
2
3
4
5
6
7
8

Fig.16.

# Response to Reviewers' Comments of ECM-D-16-00352

Ms. Ref. No.: ECM-D-16-00352
Title: Photocatalytic characteristics of CO2 reduction by CO co-feed combined with photocatalytic water splitting
Energy Conversion and Management

Dear Editor,

Thanks for your comments and suggestions on our manuscript. Those comments are all valuable and very helpful for revising and improving our paper, as well as important for guiding our researches. We have modified the manuscript accordingly and seriously. Detailed corrections are listed below point by point.

Reviewer #1:
The authors developed a simple two dimensional computational model to characterize the photocatalytic reduction of carbon dioxide by CO co-feed in a novel twin reactor. It has been demonstrated that photocatalytic CO2 reduction combined with the water splitting is viable to produce fuels at a high yield rate. More importantly, the modeling and numerical methods are verified by previous experimental work. Therefore, the results are very interesting, which may have great potential for the applications. Therefore, I think the manuscript could be accepted after the following minor issues should be addressed carefully:
1. Some typing errors should be revised carefully throughout the manuscript. For example, Line 42 on Page 6, the number in "CO2" should be the form of subscript
**Reply:** Thanks for the reviewer's comments. We have carefully checked the spelling and grammar throughout the manuscript, and corrected all the mistakes to make sure our paper more idiomatic and acceptable.

2. The following title can be referenced: "Photocatalytic reduction of CO2 by CO co-feed combined with photocatalytic water splitting in a novel twin reactor"
**Reply:** Thanks for the reviewer's comment. The proposed title is more suitable and helpful, and we have changed as the reviewer's comment in the revised manuscript.

3. Some figures can be combined together.
**Reply:** Thanks for the reviewer's suggestions. In this manuscript, some figures may contain only one curve and some points with insufficient information. We try to combine these figures together in the revised manuscript, so that more information can be presented in one figure. For example, Figs. 13, 14 and 15 have been combined to one figure, and the solar scatter plots have been deleted.

Reviewer #2:
The results provided theoretically using the proposed model is very much away from those to be produced in real experiments. The original results published for hydrogen

generation using this twin-reactor system do not provide the sufficient basis for that reaction to happen in a two-compartment cells and why the hydrogen ions should travel from water splitting compartment to $CO_2$ reducing compartment. This manuscript does not provide the essential information to make use of the information presented in this manuscript.

**Reply:** Thanks for the reviewer's comments, which can make this article more comprehensive and logical. Some theoretical basis for the reaction happening in a two-compartment cell and why the hydrogen ions should travel from water splitting compartment to $CO_2$ reducing compartment have been supplemented to the revised manuscript.

1. Why do the reactions happen in a two-compartment cell?

**Reply:** In 1987, Graetzel et al.[1] reported that with the help of $TiO_2$ nanoparticles catalyst, $CH_4$ was produced from the gas mixture of $H_2$ and $CO_2$ with the production rate of about 116μL/h. In 2007, Lo et al.[2] confirmed that the $CO_2$ photoreduction was improved by a mixture of $H_2$ and $H_2O$ compared with using solely $H_2$ or $H_2O$. Many studies on $CO_2$ hydrogenation to yield organics have been reported, which provide a theoretical basis for the chemical reactions in this paper. Moreover, the conversion of $CO_2$ into hydrocarbons is feasible from the thermodynamic viewpoint. For instance, the photoreduction of $CO_2$ to produce $CH_3OH$ can be represented by five possible reactions as shown in Table. The enthalpies ($\Delta H^0$) of all the five reactions are negative at room temperature, which proves that the reactions are exothermic. The Gibbs free energy ($\Delta G^0$) of the reactions (1), (4) and (5) are negative, meaning that the reactions are spontaneous, equilibrium favorable. Moreover, although the $\Delta G^0$ of the reactions (2) and (3) are positive, meaning that they are thermodynamically not spontaneous, those values are still much lower than that of water splitting ($\Delta H^0$= 285.8 kJ/mol;$\Delta G^0$ = 237.1 kJ/mol). Hence, the photocatalysts can convert photon energy into chemical energy accompanied by this slightly positive change in the Gibbs free energy.

Changes of enthalpy and Gibbs free energy in the $CO_2$ photoreduction reactions[3]

| Reactions | $\Delta H^0$ (kJ/mol) | $\Delta G^0$ (kJ/mol) |
|---|---|---|
| (1) $CO_2(g)+3H_2(g)\rightarrow CH_3OH(l)+H_2O(l)$ | −137.8 | −10.7 |
| (2) $CO(g)+CH_3OH(l)\rightarrow HCOOCH_3(l)$ | −25.6 | 6.6 |
| (3) $CO_2(g)+H_2(g)+CH_3OH(l)\rightarrow HCOOCH_3(l)+H_2O(l)$ | −31.8 | 25.8 |
| (4) $HCOOCH_3(l)+2H_2(g)\rightarrow 2CH_3OH(l)$ | −99.7 | −35.1 |
| (5) $HCOOCH_3(l)+CO(g)\rightarrow CH_3CHO(l)+CO_2(g)$ | −96.5 | −86.7 |

We expounded the rationality and necessity of the reaction mentioned in this paper from two points of view of past experimental research and thermodynamics, which

were added in the introduction part of the revised manuscript. More details were introduced in the references[3, 4].

2. Why should the hydrogen ions travel from water splitting compartment to $CO_2$ reducing compartment?

**Reply:** As is shown in the following figure, in the novel twin reactor, one of the key components is the modified Nafion membrane that allows not only the transport of hydrogen ions, but also the exchange of the electron mediators ($Fe^{2+}/Fe^{3+}$). The electron is shuffled via the electron mediator ($Fe^{2+}/Fe^{3+}$) through membrane. The mass and charge balances are kept concurrently by the diffusion of $H^+$ through the membrane. This information has been supplemented to the physical model of the revised manuscript. More details were introduced in the references[5].

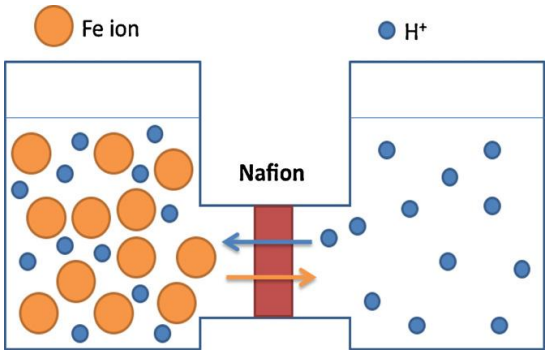


A connected twin reactor separated by a modified Nafion membrane

Reviewer #3:

1. Please add the graphical abstract.

**Reply:** Thanks for the reviewer's comment. The graphical abstract has been provided in the revised manuscript.

2. Please consider the effects of pH in the present reactor system.

**Reply:** Thanks for the reviewer's comment. When the solution contains electrolytes, electrolyte ions will reduce the solubility of gases[6]. The Henry constant of gas in pure $H_2O$ is different from that in the electrolyte solution, hence the correction coefficient of Henry constant $\varphi$ has been introduced in the reserach of Ueyama and Hatanaka [6]:

$$\begin{aligned} H &= \varphi H^0 \\ \lg \varphi &= \sum h_i V_i \end{aligned} \tag{1}$$

$H^0$ and $H$ are Henry constants for the gas in the water and electrolyte, respectively. $V_i$ is the electrolyte ionic strength calculated by Eq.(2) as follows, and $h_i$ is the reduced coefficient of solubility caused by electrolyte, which is calculated by $h=h^+ + h^- + h^*$. $h^+$, $h^-$, $h^*$ are influenced by the positive and negative ions, and the dissolved gases.

$$V_i = \frac{1}{2}\sum c_j z_j^{\,2} \tag{2}$$

Where, $c_j$ is the ion concentration, $z_j$ is the ion valence.

The electrolytes in the system are $H^+$, $Fe^{2+}$, $Fe^{3+}$, $Cl^-$ and $SO_4^{2-}$ according to the related experiments. As the physical model introduced above, the pH which has an impact on the gas dissolution process, is set as 2.6 (adjusted by adding sulfuric acid) of the solution. And in this work, $H^+$ is considered with the same electrolyte as $Fe^{2+}$, $Fe^{3+}$ and $Cl^-$, so the pH effects on the solubility of $CO_2$ are illustrated by correction coefficient $\varphi$. The aforementioned information has been supplemented to the mass transfer model in the revised manuscript. More details were introduced in the reference [6].

Additional Comment from the Editor: The English language used in this manuscript is rather weak. Can the authors get this manuscript to be proof read by a colleague that is a native English speaker or perhaps with the help of professional English editing?
**Reply:** We have done our best to revise this paper in detail and correct some languages throughout the manuscript to make sure our paper more idiomatic and acceptable. Thanks for the comments from the Editor.

**References**

[1] Thampi KR, Kiwi J, Gratzel M. Methanation and photo-methanation of carbon dioxide at room temperature and atmospheric pressure. Nature 1987;327:506-8.
[2] Lo C-C, Hung C-H, Yuan C-S, Wu J-F. Photoreduction of carbon dioxide with H2 and H2O over TiO2 and ZrO2 in a circulated photocatalytic reactor. Sol Energ Mat Sol C 2007;91:1765-74.
[3] Cheng Y-H, Nguyen V-H, Chan H-Y, Wu JCS, Wang W-H. Photo-enhanced hydrogenation of $CO_2$ to mimic photosynthesis by CO co-feed in a novel twin reactor. Appl Energ 2015;147:318-24.
[4] Lee W-H, Liao C-H, Tsai M-F, Huang C-W, Wu JCS. A novel twin reactor for $CO_2$ photoreduction to mimic artificial photosynthesis. Applied Catalysis B: Environmental 2013;132-133:445-51.
[5] Yu S-C, Huang C-W, Liao C-H, Wu JCS, Chang S-T, Chen K-H. A novel membrane reactor for separating hydrogen and oxygen in photocatalytic water splitting. J Membrane Sci 2011;382:291-9.
[6] Ueyama K, Hatanaka J. Salt effect on solubility of nonelectrolyte gases and liquids. Chem Eng Sci 1982;37:790–2.

# Photocatalytic reduction of $CO_2$ by CO co-feed combined with photocatalytic water splitting in a novel twin reactor

Shang Li[1], Lijun Yang*[1], Oluwafunmilola Ola*[2], Mercedes Maroto-Valer[2], Xiaoze Du[1], Yongping Yang[1]

*1. Key Laboratory of Condition Monitoring and Control for Power Plant Equipments of Ministry of Education,*

*School of Energy Power and Mechanical Engineering, North China Electric Power University, Beijing 102206, China*

*2. Centre for Innovation in Carbon Capture and Storage (CICCS),*

*School of Engineering and Physical Sciences, Heriot-Watt University, Edinburgh, EH14 4AS, UK*

## ABSTRACT

As a promising way to control greenhouse gas emission and alleviate global energy shortage, photocatalytic reduction of carbon dioxide attracts more attentions in recent years since it can produce fuels efficiently with the combination of $H_2$ through water splitting. In this work, a computational model which characterizes the photocatalytic

* Corresponding author: Lijun Yang. Tel: +86 10 61773373; Fax: +86 10 61773877. *E-mail address:* yanglj@ncepu.edu.cn

Oluwafunmilola Ola. Tel: +44 (0) 131 451 4737. *E-mail address:* O.O.Ola@hw.ac.uk

reduction of carbon dioxide by CO co-feed in a novel twin reactor is developed with three subsidiaries of chemical reaction kinetics, gas-liquid mass transfer, and transient sun light intensity distribution. Thanks to previous experimental work as the reliable verification for the numerical simulation, the variations of the $CH_3OH$ concentration with the $CO/CO_2$ ratio of gas mixture, pressure and temperature are obtained and analyzed. The results show that the carbon in CO can form $CH_3OH$ directly, however the excessive CO will react with $HCOOCH_3$ to form $CH_3CHO$, which results in a reduced $CH_3OH$ concentration. Besides, the $CH_3OH$ concentration subsequently increases as the temperature and pressure increase, and the $CH_3OH$ product and reaction rate vary widely with time due to the changing sun light intensity during the day.

***Key words*****:** twin reactor, $CO_2$ reduction, water splitting, photocatalysis, methanol, sun light intensity

33 **Nomenclature**

| | | |
|---|---|---|
| $c$ | concentration | $mol \cdot m^{-3}$ |
| $D$ | diffusion coefficient | $m^{2} \cdot s^{-1}$ |
| $I$ | light intensity | $W \cdot m^{-2}$ |
| $k$ | kinetic rate constant | $m^{4} \cdot s^{-1} \cdot mol^{-2}$ |
| $L$ | reactor height | mm |
| $M$ | molecular weight | $g \cdot mol^{-1}$ |
| $p$ | pressure | Pa |
| $r$ | reaction rate | $mol \cdot m^{-3} \cdot s^{-1}$ |
| $R$ | radius | mm |
| $t$ | time | s |
| $T$ | temperature | K |
| $V$ | molar volume | $cm^{3} \cdot mol^{-1}$ |
| $N$ | mass transfer rate | $mol \cdot m^{-2} \cdot s^{-1}$ |
| $K$ | mass transfer coefficient | $s \cdot mol \cdot kg^{-1} \cdot m^{-1}$ |
| $H$ | Henry constant | $Pa \cdot m^{3} \cdot mol^{-1}$ |
| $V$ | ionic strength | $mol \cdot m^{-3}$ |
| $E$ | electric field intensity | $V \cdot m^{-1}$ |
| $z$ | ionic valence | |
| $h$ | solubility coefficient | |

| | |
|---|---|
| $X$ | sun unit vector |
| $Y$ | sun unit vector |
| $Z$ | sun unit vector |
| $m$ | energy coefficient |
| $Rf$ | reflectivity |
| $Tr$ | transmissivity |
| $Ab$ | absorptivity |
| $n$ | refractivity |
| $L$ | latitude |
| $Day$ | day of year |
| $Hr$ | local solar time |

Greek letters

| | | |
|---|---|---|
| $\delta$ | film thickness | mm |
| $v$ | chemical calculated number | |
| $\rho$ | density | $kg \cdot m^{-3}$ |
| $\varphi$ | correction coefficient of Henry constant | |
| $\psi$ | proportional coefficient | S |
| $\omega$ | hour angle | |
| $\delta$ | declination | |
| $\alpha$ | solar altitude | |

| | |
|---|---|
| $\gamma$ | solar azimuth |

Subscript and superscript

| | |
|---|---|
| *A* | material |
| *B* | material |
| *F* | material |
| *O* | material |
| *a* | chemical calculated number |
| *b* | chemical calculated number |
| *f* | chemical calculated number |
| *o* | chemical calculated number |
| *L* | liquid phase |
| *G* | gas phase |
| *j* | number of reaction |
| *i* | number of reactant or ion |
| *m* | interface |
| *s* | sun |
| *x* | carbon source from carbon dioxide |
| *y* | carbon source from carbon monoxide |

35

## 1. Introduction

Since fossil fuels dominate more than 85% of energy consumption all over the world at the status quo, the rapid depletion has concentrated the growing concerns on the global energy crisis and an increasing carbon dioxide ($CO_2$) emission, which motivates researchers exploring the $CO_2$ reduction and utilization[1-5]. In the past decades, the conversion of $CO_2$ to value-added chemicals and renewable fuels has been investigated by various methods such as thermal conversion, plasma conversion and photoreduction[6]. Among various technologies of energy conservation and emission reduction[7-9], the photocatalytic $CO_2$ reduction into hydrocarbon fuels is a promising and eco-friendly method to prevent the increasing of greenhouse gases and depletion of fossil resources[5, 10, 11]. Since the first demonstration in 1979 by Inoue et al.[12], the approach of photocatalytic $CO_2$ reduction has received increasing attentions [13-15].

For the traditional photo-technology, $CO_2$ can be reduced by water ($H_2O$) to CO, $CH_4$, HCOOH, HCHO and $CH_3OH$ over semiconductor materials such as $TiO_2$, ZnO, $WO_3$, SiC, CdS, and GaP[16-19]. However, $CO_2$ is hardly reducible since $H_2O$ is a weak reductant. What's worse, the hydrocarbon products can be easily oxidized, which results in a low output ratio of hydrocarbons unexpectedly. In recent years, the technology of hydrogen production from photocatalytic water splitting has achieved a rapid progress [20, 21]. In 1987, Thampi et al.[22] reported that under the action of

$TiO_2$ nanoparticles catalyst, $CH_4$ was produced from the gas mixture of $H_2$ and $CO_2$ with the production rate of about 116μL/h. And in 2007, Lo et al.[23] confirmed that the $CO_2$ photoreduction was improved by a mixture of $H_2$ and $H_2O$ compared with that using solely $H_2$ or $H_2O$. Many studies on $CO_2$ hydrogenation to yield organics have been reported, which provide a theoretical basis for the chemical reactions of photocatalytic reduction of carbon dioxide with the combination of $H_2$ through water splitting. Twin reactor system can combine the water splitting with $CO_2$ reduction because the reducibility of $H_2$ is better than $H_2O$, so the $CO_2$ photo-reduction with $H_2$ through water splitting is more viable to produce fuels at a higher yield rate [11], as it has also been experimentally investigated in previous studies [24-26].

Twin reactor usually consists of two components for photocatalytic water splitting and photocatalytic $CO_2$ reduction, which are divided by an ion exchange unit. $H^+$ from water splitting is directly used to perform the $CO_2$ photo-hydrogenation with the participation of the light at the room temperature. The conversion of $CO_2$ into hydrocarbons is feasible from the thermodynamic viewpoint. For instance, the photoreduction of $CO_2$ to produce $CH_3OH$ can be represented by five possible reactions as listed in Table 1. The enthalpies ($\Delta H^0$) of all the five reactions are negative at room temperature, which proves that the reactions are exothermic. The Gibbs free energies ($\Delta G^0$) of the reactions (1), (4) and (5) are negative, meaning that the reactions are spontaneous, equilibrium favorable. Moreover, although the $\Delta G^0$ of

the reactions (2) and (3) are positive, meaning that they are thermodynamically not spontaneous, those values are still much lower than that of water splitting ($\Delta H^0$= 285.8 kJ/mol; $\Delta G^0$ = 237.1 kJ/mol). Hence, the photocatalysts can convert photon energy into chemical energy accompanied by this slightly positive change in the Gibbs free energy[25]. The combination of photocatalytic $CO_2$ reduction with water splitting in the twin rector presents a better performance than the $CO_2$ reduction by $H_2O$, and prevents the oxygenation of hydrocarbon products.

CO was considered as a co-feed to enhance the production efficiency of $CH_3OH$, and a certain amount of CO mixed with the reaction gases can promote $CH_3OH$ production under the same conditions because CO is thermodynamically more favorable as compared to the $CO_2$. However, due to the limitation of experimental conditions, it did not address how the CO affects the methanol production. When the reaction gas is pure CO, $CH_3OH$ cannot be produced, which was not clarified in detail by previous studies. Other operating conditions such as the pressure and temperature in the twin reactor, which are crucial to the photocatalytic reduction of $CO_2$, were also not deeply investigated. What's more, there are few related studies about the sun light effect on the photocatalytic $CO_2$ reduction in twin reactors, since most of the experiments were carried out in an indoor environment with the artificial light instead of natural sources. Adopting the software SOLTRACE in this work, the principle of CO effect on the $CH_3OH$ production and the impacts of operation conditions on the

conversion efficiency from $CO_2$ to $CH_3OH$ in the twin reactor are deeply investigated by unveiling the sun light distribution as well as the photocatalytic $CO_2$ reduction mechanism. It can be of benefit to the optimal design and operation of twin reactors by investigating the photocatalytic reduction of $CO_2$ by CO co-feed combined with photocatalytic water splitting.

## 2. Model development

### *2.1 Physical model*

The physical model of the twin reactor can be simplified as Fig.1, which has been described in detail and experimentally investigated in some of the photocatalytic characteristics [24-26]. With a Nafion membrane for segregation, 0.15 g of $Pt/CuAlGaO_4$ and 0.15 g of $Pt/SrTiO_3$:Rh in 2mM $FeCl_2$ were placed in the $CO_2$ reduction reactor solution, while 0.30 g of commercial $WO_3$ in 2mM $FeCl_3$ solution were put in the water splitting reactor. In the novel twin reactor, one of the key components is the modified Nafion membrane that allows not only the transport of hydrogen ions, but also the exchange of the electron mediators ($Fe^{2+}/Fe^{3+}$). The electron is shuffled via the electron mediator ($Fe^{2+}/Fe^{3+}$) through membrane. The mass and charge balances are kept concurrently by the diffusion of $H^+$ through the membrane[27]. The pH of the solution is 2.6 (adjusted by adding sulfuric acid) and the volume of each compartment of the twin reactor is 225 mL. The $H^+$ generated by $H_2O$ splitting goes through the Nafion membrane and forms $H_2$, which reacts with

$CO_2$ to produce organic compounds. In this work, the multi-physics coupling software is used to simulate the above process with the following necessary assumptions, based on which the model can be well simplified without introducing unexpected errors.

1) Since the driving force of the photoreaction originates from the light energy but not the thermal energy (i.e. molecular kinetics at high temperatures) in the traditional catalytic reaction, most photoreactions work at about the room temperature. As a result, the thermodynamic effects of the reactions at various temperatures can be ignored because of the extremely weak provoking energy in the photocatalysis.
2) Thanks to the magnetic stirrer in the experiment for the uniform catalyst distribution in the solution, the reaction rate is assumed to be a function of the time rather than the location.
3) Since CO and $CO_2$ are free from liquidation at the room temperature and atmospheric pressure, the mixture can be seen as an ideal gas so as to easily calculate the partial pressure based on the ideal gas equation. Besides, the chemical process at the interface of the gas and liquid is not taken into account.
4) The effects of the catalyst surface topography, concentration, band gap, and absorption or desorption existing on the surface of catalyst particles are ignored.
5) The chemical reactions in the twin reactor take the following forms, which are regarded as single step reactions [25].

$$h\nu \xrightarrow{UV,photocatalyst} h^+ + e^-$$

$$H_2O + 2h^+ \xrightarrow{UV,photocatalyst} 2H^+ + \frac{1}{2}O_2$$

$$2H^+ + 2e^- \xrightarrow{UV,photocatalyst} H_2$$

$$CO_2 + 6H^+ + 6e^- \xrightarrow{UV,photocatalyst} CH_3OH + H_2O$$

$$CH_3OH + CO \xrightarrow{UV,photocatalyst} HCOOCH_3$$

$$CH_3OH + CO_2 + 2H^+ + 2e^- \xrightarrow{UV,photocatalyst} HCOOCH_3 + H_2O$$

$$HCOOCH_3 + CO \xrightarrow{UV,photocatalyst} CH_3CHO + CO_2$$

$$HCOOCH_3 + 4H^+ + 4e^- \xrightarrow{UV,photocatalyst} CH_3OH$$

$$H_2O + CO \xrightarrow{UV,photocatalyst} H_2 + CO_2$$

With the aforementioned equations, the inferior middle processes are reasonably ignored for clearly uncovering the chemical mechanism from the reactants to products.

*2.2 Chemical reaction kinetics model*

For the chemical reaction aA+bB=fF+oO under constant volume conditions, the reaction rate can be expressed as follows:

$$r = -\frac{1}{a}\frac{dc_A}{dt} = -\frac{1}{b}\frac{dc_B}{dt} = \frac{1}{f}\frac{dc_F}{dt} = \frac{1}{o}\frac{dc_O}{dt} \quad (1)$$

When the reaction is an elementary reaction, the above formula can be written as:

$$r = kc_A{}^a c_B{}^b \quad (2)$$

Where $k$ is the reaction rate constant.

In previous studies, it has been noticed that the photocatalytic reaction rate follows a power law expression of the light intensity[28]. By experimental studies, Herrmann suggested that the reaction rate is proportional to the light intensity at low light

intensities, and when the light intensity is high, the reaction rate is proportional to the square root of the light intensity [29]. According to the work of Wang et al., the photocatalytic reaction rate was considered proportional to the n-th power of the light intensity[17], where n is a factor to describe the reaction rate dependency on light irradiance. The higher n value of the reactor represents that the incident photons can be more effectively utilized for photocatalytic reactions[30]. Therefore, the reversible catalytic reaction rate equation can be written with the following form:

$$r_j = I^m \left( k_j \prod_{i=1} c_i^{\nu_i} \right) \tag{3}$$

Where $r_j$ is the reaction rate, $k_j$ is the kinetic rate constant, $c_i$ is the concentration, $\nu_i$ is the chemical calculated number, $I$ is the light intensity, $m$ is the energy coefficient.

*2.3 Mass transfer model*

Many physical models, such as two-film, Higbie penetration, Danckwerts surface renewal and turbulent mass transfer theories, all formerly clarified the process of gas-liquid mass transfer. With two-film theory adopted in this work, a static film on each side of the gas-liquid interface is assumed as the gas membrane and liquid membrane. Moreover, the mass transfer rate of gas-liquid interphase depends on the diffusion rate of gas and liquid membranes.

$$N = \frac{D_G}{RT\delta_G}(p_G - p_m) = \frac{D_L}{\delta_L}(c_m - c_L) \tag{4}$$

Where $N$ is the mass transfer rate, $D_G$ and $D_L$ are the diffusion coefficients of components in gases and liquids respectively. $\delta_G$ and $\delta_L$ are the gas and liquid film thicknesses, which are about 0.1mm according to the experiment. $c_m$ and $p_m$ represent

the concentration and partial pressure at the interface of the membranes. $p_G$ is the partial pressure of components in gas phase while $c_L$ is the concentration of components in liquid phase. $R$ is the perfect gas constant and $T$ is temperature.

By eliminating the interface concentration $c_m$ and the interface pressure $p_m$ in the above formula, the mass transfer rate is expressed as:

$$N = K_G(p_G - p^*) = K_L(c^* - c_L)$$
$$p^* = Hc_L; c^* = \frac{p_G}{H} \tag{5}$$

Where $p^*$ is the partial pressure in equilibrium with $c_L$, $c^*$ is the concentration in equilibrium with $p_G$, $H$ is the Henry constant, $K_G$ and $K_L$ represent gas phase total mass transfer coefficient and liquid phase total mass transfer coefficient:

$$K_G = \frac{1}{\frac{RT\delta_G}{D_G} + \frac{H\delta_L}{D_L}}$$
$$K_L = \frac{1}{\frac{RT\delta_G}{HD_G} + \frac{\delta_L}{D_L}} \tag{6}$$

When the solution contains electrolytes, electrolyte ions will reduce the solubility of gases[31]. The Henry constant of gas in pure $H_2O$ is different from that in the electrolyte solution, hence the correction coefficient of Henry constant $\varphi$ has been introduced in the research of Ueyama and Hatanaka [31]:

$$H = \varphi H^0$$
$$\lg \varphi = \sum h_i V_i \tag{7}$$

$H^0$ and $H$ are Henry constants for the gas in the water and electrolyte, respectively. $V_i$ is the electrolyte ionic strength calculated by Eq.(8) as followed, and $h_i$ is the reduced coefficient of solubility caused by electrolyte, which is calculated by $h=h^+ + h^- + h^*$. $h^+$,

$h^-$, $h^*$ are influenced by the positive and negative ions, and the dissolved gases.

$$V_i = \frac{1}{2}\sum c_j z_j^{\ 2} \tag{8}$$

Where, $c_j$ is the ion concentration, $z_j$ is the ion valence.

The electrolytes in the system are $H^+$, $Fe^{2+}$, $Fe^{3+}$, $Cl^-$ and $SO_4^{2-}$ according to the related experiments.

As the physical model introduced above, the pH which has an impact on gas dissolution process, is set as 2.6 (adjusted by adding sulfuric acid) of the solution. In this work, $H^+$ is considered with the same electrolyte as $Fe^{2+}$, $Fe^{3+}$ and $Cl^-$, so the pH effects on the solubility of $CO_2$ are illustrated by the correction coefficient $\varphi$.

Diffusion coefficients of $CO_2$ in the mixed gas and the solution can be calculated according to the following formula [32, 33]:

$$\log D_L = -8.1764 + \frac{712.5}{T} - \frac{2.591\times10^5}{T^2}$$
$$D_G = \frac{435.7T^{3/2}}{P(V_A^{1/3} + V_B^{1/3})^2}\sqrt{\frac{1}{M_A} + \frac{1}{M_B}} \tag{9}$$

Where $A$, $B$ are two kinds of gas in the reactor, $p$ is the total pressure, $T$ is the temperature in the reactor and equals to 293K and $M$ is the molar mass of the gas. $V$ is the molar volume with the constant of 22.4 L/mol, due to the fact that the $CO_2$ and CO are ideal gases in the reactor.

*2.4 Sun light model*

Since the photocatalytic $CO_2$ reduction cannot work without sun light input in the twin reactor, most of the experiments were carried out in an indoor environment with

the artificial light for substitute. Unfortunately, few related studies emphasized on the sun light distribution. While in this work, with the software SOLTRACE based on the theory from Spencer and Murty[34], the sun light distribution is obtained and analyzed for its optical performance, which is highly affected by the light diffusion as a key factor that can be predicted by setting up accurate parameters in SOLTRACE.

The angular intensity distribution and position of the light together define the natural energy source, and in Beijing (northern latitude 40°5', east longitude 116°16'), the 200nd day during the year with the maximum sun declination is usually selected for sunlight acquisition. Although the Gaussian and Pillbox apparatus can together determine the sun shape, it cannot represent the real sunlight condition due to the complex atmospheric factors as well as inevitable errors from the optical equipment. Since the Gaussian leads to an obviously higher error than pillbox, it is dismissed in this paper. The sunlight position ($X_s$, $Y_s$, $Z_s$) can be calculated by latitude ($L$: +N, -S), day of year ($Day$) and local solar time ($Hr$) as follows.

$$\begin{aligned} X_s &= sin\gamma_s cos\alpha_s \\ Y_s &= sin\alpha_s \\ Z_s &= cos\gamma_s cos\alpha_s \end{aligned} \tag{10}$$

Where $\alpha_s$ is the solar altitude and $\gamma_s$ is the solar azimuth, which can be obtained by the following form.

$$\begin{aligned} \alpha_s &= \sin^{-1}(\cos L \cos\delta \cos\omega + \sin L \sin\delta) \\ \gamma_s &= \cos^{-1}[\frac{\sin\alpha_s \sin L - \sin\delta}{\cos\alpha_s \cos L}] \end{aligned} \tag{11}$$

Where $\omega$ is the hour angle, $\omega$=15(*Hr*-12). *Hr* is the local solar time, which is set from 8:00 to 16:00. $\delta$ is the declination, $\delta$= 23.45sin (360(284+*Day*)/365). *Day* is set as 200, implying the maximum sun declination, and *L* as 40°5', representing the latitude of Beijing.

Optical properties can be obtained from the movement of rays when they hit the surfaces. According to the experiment of Chen et al.[25], the body of the reactor is made of glass which can be treated as fully transparent, so the absorptivity is set to 0. The reflectivity and the transmissivity of the twin reactor can be obtained by the following forms.

$$Rf = \frac{(n_1 - n_2)}{(n_1 + n_2)} \qquad (12)$$
$$Rf + Tr = 1$$

Where *Rf* is reflectivity, *Tr* is transmissivity, *n* is refractivity that can be obtained from the relevant literature. In addition, due to the effect of the element surface shape on ray direction, surface slope error and surface specularity can be included, which together affect ray interaction at the surface in a combined form as follows

$$\sigma_{\text{optical}} = (4\sigma^2{}_{\text{slope}} + \sigma^2{}_{\text{specularity}})^{1/2} \qquad (13)$$

Where $\sigma_{\text{optical}}$ is the comprehensive factor, $\sigma_{\text{slope}}$ means the surface slope error, and $\sigma_{\text{specularity}}$ represents the surface specularity error.

*2.5 Evaluation of model parameters*

The variables and constants used in this model are listed in Table 2 with specific

meanings. The geometric parameters were obtained based on the real dimensions of the reactor and the kinetics parameters by fitting the experimental data. Since the reaction rate constant is not known in advance, should it be assumed at first. The $CH_3OH$ production can be numerically calculated and then compared with the experimental data. If the error is not within the allowed value, should the reaction rate constant as aforementioned above be reassumed for expecting results. The mass transfer parameters were estimated by Eqs.(7-9) with the initials referring to the experiment, and the sun position parameters by Eqs.(10) and (11) with the optical variables determined by Eqs.(12) and (13).

*2.6 Validation of numerical results*

Adopting the reaction engineering and diluted species transport modules, Eqs.(2-3) and (4-9) can be solved respectively by the commercial software COMSOL. Besides, the reaction rate can be iterated as the light intensity was taken into account by setting global variables.

The initial conditions with pure $CO_2$ are simulated as shown in Figs. 2 and 3. As observed, the $H_2$ concentration increases sharply at the beginning since the $H^+$ generated by water decomposition penetrates directly through the ion exchange membrane to form $H_2$. Meanwhile, the $O_2$ concentration in the water splitting reactor also rises with a half production of $H_2$. However as the $O_2$ increases stably, the $H_2$ in the $CO_2$ reduction reactor no longer increases and keeps at the rate of nearly

0.85μmol/g, showing that $H_2$ already reaches a balance since it generated by water splitting transforms directly into the $CH_3OH$ and other organic compounds. So at the beginning five hours, even the increasing rate declines gradually, the $CH_3OH$ rises conspicuously with an average speed of 0.8 μmol/g/h, while it then keeps almost no change with the ultimate concentration of 4μmol/g as shown in Fig. 3. Besides, Fig. 3 shows that the average error between the simulation and experimental results is about 13.12%, which is quite small. Moreover, Fig. 4 shows the concentration of methyl formate ($HCOOCH_3$) and acetaldehyde ($CH_3CHO$) as the two by-products during the reaction process, which reaches 1.5μmol/g and 0.4 μmol/g with the average rate of 0.1875 μmol/g/h and 0.05 μmol/g/h respectively within the 8 hours. The $CO_2$ and CO composite process is also numerically calculated with the initial partial pressure of CO set in accordance with the mixing ratio of 1:10 and 1:5 respectively as shown in Figs. 5 and 6, which clearly present that the final $CH_3OH$ concentrations are 7.8 μmol/g and 7.4μmol/g after 8 hours with the relative errors between the simulating and experimental results of 4.41% and 2.92% respectively.

The comparisons show that the numerical and experimental results agree well with each other, so the modelling approach is reliable and accurate enough to predict the photocatalytic $CO_2$ reduction performances in the twin reactor system. Since the photocatalytic $CO_2$ reduction gradually recedes with an ultimately constant $CH_3OH$ concentration, the working conditions of the twin reactor system can be optimized by

means of numerical simulations.

## 3. Results and discussion

### *3.1 Effects of gas mixture ratio*

Pure CO as the reactant gas is specifically simulated so as to unveil its characteristics during the overall process at the ambient pressure and temperature of 1atm and 293K respectively. Fig. 7 shows that the $H_2$ presents almost twice the concentration of $O_2$, while the $CH_3OH$ concentration displays nearly zero due to the non-conversion from hydrogen, which clearly shows the unavailable direct chemical reaction between the pure CO and hydrogen or hydrogen ions. However, very small amount of $CH_3OH$ (less than 0.1μmol/g) exists inevitably due to the following reaction in the reduction reactor:

$$H_2O+CO \xrightarrow{UV,photocatalyst} H_2+CO_2$$
$$CO_2+6H^++6e^- \xrightarrow{UV,photocatalyst} CH_3OH+H_2O$$

The overall process at various gas mixture ratios of CO to $CO_2$ was numerically simulated during the whole 20 hours with the carbon elements symbolized as $C_x$ from $CO_2$ and $C_y$ from CO for easy analysis of the carbon trails existing in methanol. Fig.8 displays the processing amount of $C_xH_3OH$ as well as $C_yH_3OH$ at the CO to $CO_2$ ratio of 1:10. During the first 8 hours, it can be observed that the $C_xH_3OH$ has a higher production rate of 0.53 μmol/g/h, while only 0.45 μmol/g/h for the $C_yH_3OH$. After then, it changes little for the concentration of $C_xH_3OH$ with a stable amount of 4.2μmol/g at the 20th hour. But for $C_yH_3OH$, the concentration always increases and

eventually reaches about 4.6 μmol /g after 20 hours. It shows that the CO can easily transform into the methanol and other organic compounds through the chemical chains as aforementioned above compared with $CO_2$. As shown in Fig. 9, the production of $C_xH_3OH$ declines with the CO to $CO_2$ ratio of 1:5 compared with the case of 1:10, and only arrives at 3.6μmol/g for the maximum concentration. As for $C_yH_3OH$, the concentration reaches the peak of nearly 3.75 μmol/g at the time of 7.5h, then it decreases to 2.1 μmol /g after 20 hours and finally presents a declining tendency. Since CO plays a double role during the $CH_3OH$ production, may the $CH_3OH$ increase due to its positive effect with a small amount, while should other organic compounds unexpectedly emerge with an excessive CO ratio. Fig. 10 shows the $CH_3CHO$ concentration at various gas mixture ratios, which clearly presents the always small value less than 0.5 μmol/g at the first 5 hours. But the $CH_3CHO$ production rate increases as the chemical process continues, and it presents a higher value at a more intensive CO concentration. Besides, as the ratio of CO to $CO_2$ changes from 1/20 to 1/2, the $CH_3CHO$ concentration increases from 1.5 μmol/g to 3.75 μmol/g after 20 hours.

Figs.8-10 fully explain the mechanisms of the CO dominance in the photocatalytic process, which can be described by the following three reactions.

$$(1)\quad CH_3OH+CO \xrightarrow{UV,photocatalyst} HCOOCH_3$$

$$(2)\quad HCOOCH_3+CO \xrightarrow{UV,photocatalyst} CH_3CHO+CO_2$$

$$(3)\quad HCOOCH_3+4H^+ +4e^- \xrightarrow{UV,photocatalyst} 2CH_3OH$$

When a small amount of CO gas exists in the reactor, the CO reacts with $CH_3OH$ to form $HCOOCH_3$ as reaction (1). Due to the excessive $H_2$, the $HCOOCH_3$ reacts with $H_2$ and then generates $CH_3OH$ as reaction (3). In this case, the CO promotes $CH_3OH$ production. However, if CO gas is excessive, the CO will react with $CH_3OH$ to form $HCOOCH_3$ at first, then the remaining CO continues to react with $HCOOCH_3$ to produce $CH_3CHO$ as reaction (2), which prevents $HCOOCH_3$ from reacting with $H_2$, resulting in an indirect consumption of $CH_3OH$.

The aforementioned conclusion about the gas mixture ratio can be of benefit to the design and application of photocatalytic reactor systems. For the twin reactor, the optimal CO to $CO_2$ ratio as well as reaction time can be recommended with reference to the light intensity distribution and reactor structure. Moreover, increasing the byproduct of $CH_3CHO$ during the photocatalytic process proves efficient to prevent the side effect as reaction (2).

*3.2 Effects of pressure*

The mixture pressure in the reactor is of great importance for photocatalytic reactions. According to Henry's law, the partial pressure of the mixture above the liquid surface can directly affect the gas solubility. Besides, the mass transfer rate between the gas and liquid is related greatly with the partial pressure in terms of the two-film theory. Fig. 11 presents the production of $CH_3OH$ at various pressures during the 20 hours. It can be seen that as the initial pressure in the reactor goes up,

346 the $CH_3OH$ yield increases. When the initial pressure reaches 20atm, the $CH_3OH$
347 concentration arrives at 14.5 μmol/g at 20 hours, which is 52.6% higher than that of
348 9.5 μmol/g at the initial pressure of 1atm. As for the efficiency, increasing the initial
349 pressure in the reactor will consume more energy, so a viable operating pressure
350 should be determined for the photocatalytic reactor in potential engineering
351 applications.

352 *3.3 Effects of temperature*

353 The Henry constant can well represent the solubility of $CO_2$ and CO in the
354 electrolyte. As observed from Table 3, the Henry constant increases as the temperature
355 rises. Besides, the diffusion coefficients of the gas-gas as well as gas-liquid depend
356 also upon the temperature according to Eq.(9), so the mass transfer correlates strongly
357 with the temperature. Fig.12 shows the $CH_3OH$ concentration change at various
358 temperatures, from which can be seen that the $CH_3OH$ concentration increases with
359 increasing the temperature, resulting from the comprehensive effects of the solubility
360 and mass transfer rate. At the temperature of 273K, the ultimate $CH_3OH$ concentration
361 at the 20th hour is 6 μmol/g, while at 333K it approaches 11μmol/g, presenting an
362 increase of 83.2%, which shows that the conversion efficiency can be greatly
363 improved by increasing the temperature.

364 *3.4 Effects of light intensity*

365 Based on the optical parameters of the physical model aforementioned, the sun

366 light model is developed and the two dimensional distribution of light intensity on a
367 cross-section of the reactor is achieved by adopting the software SOLTRACE. Fig. 13
368 shows transient solar flux distribution in the reactor at 8:00, 12:00 and 16:00
369 respectively, in which the positive direction of the X-axis stands for the west of the
370 reactor and the positive direction of the Y-axis represents the zenith of the twin reactor.
371 The distribution of light intensity at 8:00 is shown in Fig.13(a), which presents a
372 non-uniform light intensity scattering in the reactor with 832W/$m^2$ on the east side
373 while only 205W/$m^2$ on the west side, and the average light intensity is about
374 331W/$m^2$. As observed from Fig. 13(b), the reactor receives the sunlight vertically at
375 12:00, so the light intensity arrives at the maximum value in the center while
376 minimum value at both sides, due to the combined effects of the reflection and
377 refraction by the glass container and colored solution with the iron ion. The average
378 light intensity can reach nearly 620W/$m^2$ in the reactor. Fig. 13(c) presents the
379 irradiation at 16:00 from the west side of the reactor with the average light intensity of
380 330W/$m^2$.

381 From 8:00 to 16:00, the average light intensity is obtained and shown in Fig.14,
382 which is fitted to the following equation:

383 $$I=-1996+435Hr-18Hr^2 \quad (14)$$

384 It can be seen from Fig.14 that the results from the fitting curve agree well with the
385 simulated data, so the fitting equation is reliable enough to predict the average light

intensity change over time. Together with the chemical reaction engineering module, the photocatalytic $CO_2$ reduction combined with the water splitting process can be numerically simulated within the 8 hours (8:00-16:00) at the temperature of 293K and pressure of 1atm. Fig.15 shows the concentration changes of $O_2$, $H_2$ and $CH_3OH$ over time, proving that the $CH_3OH$ product using the sun light source is less than that using the artificial light source in the experiment of Cheng et al.[25]. As also clearly presented, the $CH_3OH$ concentration reaches the climax of 4.6 μmol/g about 3.5 hours later (11:30), and then it begins to decrease gradually due to the weakened light intensity. Fig. 16 shows the reaction rates of the photocatalytic $CO_2$ reduction and water splitting process. It can be seen that as the light intensity decreases, the photocatalytic water splitting reaction becomes slow, resulting in the reduced $H_2$ for $CO_2$ reduction. The $CH_3OH$ generating rate is lower than the consuming rate of side reaction, leading to a reduced $CH_3OH$ concentration.

Since the experimental study with the artificially unchanged light intensity could not totally represent the photocatalytic $CO_2$ reduction mechanism, the numerical method with the natural sunlight changing over time demonstrates an attractive superiority, which is closer to the real chemical process.

## 4. Conclusions

The photocatalytic reduction of $CO_2$ by CO co-feed combined with photocatalytic water splitting in a novel twin reactor was modeled and numerically investigated.

The $CH_3OH$ concentration almost linearly increases with increasing the gas mixture ratio of CO to $CO_2$, due to the direct conversion from CO to $CH_3OH$. However, the excessive CO will react with $HCOOCH_3$ to form $CH_3CHO$ unexpectedly, resulting in a reduced $CH_3OH$ concentration. Besides, with the temperature and pressure increase, the $CH_3OH$ production rises owing to the enhanced mass transfer.

The numerical method with the natural sunlight in this work proves a more accurate photocatalytic $CO_2$ reduction process compared with the experiment, and the yield of $CH_3OH$ is reduced due to the changing light intensity. It suggests the artificial light intensity adjusted with time in the photocatalytic experiment, so as to obtain a more reliable result.

**Acknowledgment**

The financial support for this research from the National Natural Science Foundation of China (Grant No. 50776032) is gratefully acknowledged. The authors also thank the support provided by the Royal Society International Project of UK (IE150489).

## References


[1] Baran T, Wojtyła S, Dibenedetto A, Aresta M, Macyk W. Zinc sulfide functionalized with ruthenium nanoparticles for photocatalytic reduction of $CO_2$. Applied Catalysis B: Environmental 2015;178:170-6.

[2] Huang Q, Yu J, Cao S, Cui C, Cheng B. Efficient photocatalytic reduction of $CO_2$ by amine-functionalized g-$C_3N_4$. Appl Surf Sci 2015;358:350-5.

[3] Tahir B, Tahir M, Amin NS. Gold–indium modified $TiO_2$ nanocatalysts for photocatalytic $CO_2$ reduction with $H_2$ as reductant in a monolith photoreactor. Appl Surf Sci 2015;338:1-14.

[4] Yuan K, Yang L, Du X, Yang Y. Performance analysis of photocatalytic $CO_2$ reduction in optical fiber monolith reactor with multiple inverse lights. Energ Convers Manage 2014;81:98-105.

[5] Yuan K, Yang L, Du X, Yang Y. Numerical analysis of photocatalytic $CO_2$ reduction in optical fiber monolith reactor with optimized structures. Energ Convers Manage 2014;87:258-66.

[6] Tahir M, Amin NS. Recycling of carbon dioxide to renewable fuels by photocatalysis: Prospects and challenges. Renewable and Sustainable Energy Reviews 2013;25:560-79.

[7] Chiu FP, Kuo HI, Chen CC, Hsu CS. The energy price equivalence of carbon taxes and emissions trading—Theory and evidence. Appl Energ 2015;160:164-71.

[8] Liu Y, Zhou Y, Wu W. Assessing the impact of population, income and technology on energy consumption and industrial pollutant emissions in China. Appl Energ 2015;155:904-17.

[9] Wang Q, Su B, Sun J, Zhou P, Zhou D. Measurement and decomposition of energy-saving and emissions reduction performance in Chinese cities. Appl Energ 2015;151:85-92.

[10] Sim LC, Leong KH, Saravanan P, Ibrahim S. Rapid thermal reduced graphene oxide/Pt-$TiO_2$ nanotube arrays for enhanced visible-light-driven photocatalytic reduction of $CO_2$. Appl Surf Sci 2015.

[11] Tahir M, Amin NS. Photocatalytic $CO_2$ reduction with $H_2$ as reductant over copper and indium co-doped $TiO_2$ nanocatalysts in a monolith photoreactor. Applied Catalysis A: General 2015;493:90-102.

[12] Inoue T, Fujishima A, Satoshi K, Honda K. Photoelectrocatalytic reduction of carbon dioxide in aqueous suspensions of semiconductor powders. Nature 1979;277:637-8.

[13] Tahir M, Amin NS. Advances in visible light responsive titanium oxide-based photocatalysts for $CO_2$ conversion to hydrocarbon fuels. Energ Convers Manage 2013;76:194-214.

[14] Broberg Viklund S, Johansson MT. Technologies for utilization of industrial excess heat: Potentials for energy recovery and $CO_2$ emission reduction. Energ Convers Manage 2014;77:369-79.

[15] Jain S, Vardia J, Ameta R, Ameta SC. Use of malachite green as photocatalyst in reduction of sodium and potassium carbonates. Energ Convers Manage 2004;45:1233-42.

[16] Tahir B, Tahir M, Amin NS. Performance analysis of monolith photoreactor for $CO_2$ reduction with $H_2$. Energ Convers Manage 2015;90:272-81.

[17] Wang T, Yang L, Du X, Yang Y. Numerical investigation on $CO_2$ photocatalytic reduction in optical fiber monolith reactor. Energ Convers Manage 2013;65:299-307.

[18] Ola O, Maroto-Valer MM. Transition metal oxide based $TiO_2$ nanoparticles for visible light induced $CO_2$ photoreduction. Applied Catalysis A: General 2015;502:114-21.

[19] Ola O, Maroto-Valer MM. Review of material design and reactor engineering on $TiO_2$

photocatalysis for $CO_2$ reduction. Journal of Photochemistry and Photobiology C: Photochemistry Reviews 2015;24:16-42.

[20] Nong G, Chen Y, Li M, Zhou Z. Generation of hydrogen free radicals from water for fuels by electric field induction. Energ Convers Manage 2015;105:545-51.

[21] Waskasi MM, Hashemianzadeh SM, Mostajabi Sarhangi O, Harzandi AP. Computational model of hydrogen production by Coumarin-dye-sensitized water splitting to absorb the visible light in a local electric field. Energ Convers Manage 2012;62:154-64.

[22] Thampi KR, Kiwi J, Gratzel M. Methanation and photo-methanation of carbon dioxide at room temperature and atmospheric pressure. Nature 1987;327:506-8.

[23] Lo CC, Hung CH, Yuan CS, Wu JF. Photoreduction of carbon dioxide with $H_2$ and $H_2O$ over $TiO_2$ and $ZrO_2$ in a circulated photocatalytic reactor. Sol Energ Mat Sol C 2007;91:1765-74.

[24] Shinichi I, Ryota D. Hydrogen production from water and conversion of carbon dioxide to useful chemicals by room temperature photoelectrocatalysis. Catal Today 1996;27:271-7.

[25] Cheng YH, Nguyen VH, Chan HY, Wu JCS, Wang WH. Photo-enhanced hydrogenation of $CO_2$ to mimic photosynthesis by CO co-feed in a novel twin reactor. Appl Energ 2015;147:318-24.

[26] Lee WH, Liao CH, Tsai MF, Huang CW, Wu JCS. A novel twin reactor for $CO_2$ photoreduction to mimic artificial photosynthesis. Applied Catalysis B: Environmental 2013;132-133:445-51.

[27] Yu SC, Huang CW, Liao CH, Wu JCS, Chang ST, Chen KH. A novel membrane reactor for separating hydrogen and oxygen in photocatalytic water splitting. J Membrane Sci 2011;382:291-9.

[28] Lin H, Valsaraj K. An optical fiber monolith reactor for photocatalytic wastewater treatment. Aiche J 2006:2271-80.

[29] Herrmann JM. Heterogeneous photocatalysis: an emerging discipline involving multiphase systems. Catal Today 1995;24:157-64.

[30] Denny F, Scott J, Peng GD, Amal R. Channelled optical fibre photoreactor for improved air quality control. Chem Eng Sci 2010;65:882-9.

[31] Ueyama K, Hatanaka J. Salt effect on solubility of nonelectrolyte gases and liquids. Chem Eng Sci 1982;37:790–2.

[32] Ryszard P, Wadysaw M. Kinetics of Reaction Between Carbon-Dioxide and Hydroxyl Ions in Aqueous-Electrolyte Solutions. Chem Eng Sci 1988;43:1677-84.

[33] Rathore M, Kapuno R. Engineering heat transfer: Jones & Bartlett; 2011.

[34] Spencer GH, Murty M. General Ray-Tracing Procedure. Journal of the Optical Society of America 1962;52:672-8.

**Table 1**

Changes of enthalpy and Gibbs free energy in the $CO_2$ photoreduction reactions[25].

| Reactions | $\Delta H^0$ (kJ/mol) | $\Delta G^0$ (kJ/mol) |
|---|---|---|
| (1) $CO_2(g)+3H_2(g)\rightarrow CH_3OH(l)+H_2O(l)$ | −137.8 | −10.7 |
| (2) $CO(g)+CH_3OH(l)\rightarrow HCOOCH_3(l)$ | −25.6 | 6.6 |
| (3) $CO_2(g)+H_2(g)+CH_3OH(l)\rightarrow HCOOCH_3(l)+H_2O(l)$ | −31.8 | 25.8 |
| (4) $HCOOCH_3(l)+2H_2(g)\rightarrow 2CH_3OH(l)$ | −99.7 | −35.1 |
| (5) $HCOOCH_3(l)+CO(g)\rightarrow CH_3CHO(l)+CO_2(g)$ | −96.5 | −86.7 |

**Table 2**

Model parameters for photocatalytic $CO_2$ reduction by CO co-feed.

| Type | Variables | Values | Unit |
|---|---|---|---|
| kinetics | $k_1$ | 3.3E-9 | $m^3/(s \cdot mol)$ |
| | $k_2$ | 1.7E-2 | $m^9/(s \cdot mol^3)$ |
| | $k_3$ | 2.3E-4 | $m^3/(s \cdot mol)$ |
| | $k_4$ | 1.7E-4 | $m^3/(s \cdot mol)$ |
| | $k_5$ | 5.8E-6 | $m^6/(s \cdot mol^2)$ |
| | $k_6$ | 8.1E-3 | $m^3/(s \cdot mol)$ |
| Geometry | $L$ | 11.46 | cm |
| | $R_1$ | 5 | cm |
| | $R_2$ | 4 | cm |
| Mass transfer | $D_L$ | 1.9809E-9 | $m^2/s$ |
| | $D_G$ | 1.41E-7 | $m^2/s$ |
| | $\delta_G$ | 0.1 | mm |
| | $\delta_L$ | 0.1 | mm |
| | $h_{H^+}$ | 0 | |
| | $h_{Fe^{2+}}$ | 0.049 | |
| | $h_{Fe^{3+}}$ | 0.054 | |
| | $h_{SO_4^{2-}}$ | 0.029 | |
| | $h_{Cl^-}$ | 0.021 | |

| | | | |
|---|---|---|---|
| | $h_{CO^2}$ | -0.019 | |
| | $h_{CO}$ | 0.0283 | |
| | $H_{0CO}$ | 5.43E+6 | kPa |
| | $H_{0CO_2}$ | 1.44E+5 | kPa |
| Initial value | $C_{CO_2}$ | 30.73 | $mol/m^3$ |
| | $C_{CO}$ | 0.095 | $mol/m^3$ |
| | $C_{SO_4^{2-}}$ | 1.21 | $mol/m^3$ |
| | $C_{Fe^{2+}}$ | 8.8 | $mol/m^3$ |
| | $C_{Fe^{3+}}$ | 8.8 | $mol/m^3$ |
| | $I$ | 900 | $W/m^2$ |
| | $m$ | 1 | |
| Sun position | *Day* | 200 | |
| | *Hr* | 8-16 | |
| | $L$ | 40°5’ | |
| | *Shape* | Pillbox | |
| Optical property | $Rf_{glass}$ | 0.05 | |
| | $Tr_{glass}$ | 0.95 | |
| | $Ab_{glass}$ | 0 | |
| | $n_{glass}$ | 1.6 | |
| | $Rf_{solution}$ | 0.2 | |

| | |
|---|---|
| $Tr_{solution}$ | 0.48 |
| $Ab_{solution}$ | 0.32 |
| $n_{solution}$ | 1.3 |
| *Slope error(mrad)* | 3.5 |
| *Specularity error(mrad)* | 0.2 |

**Table 3**

Henry constants at various temperatures.

| *T*(K) / Gas | 273 | 278 | 283 | 288 | 293 | 298 | 303 | 308 | 313 | 318 | 323 | 333 |
|---|---|---|---|---|---|---|---|---|---|---|---|---|
| CO ($H_x$×$10^{-6}$ kPa) | 3.57 | 4.01 | 4.48 | 4.95 | 5.43 | 5.88 | 6.28 | 6.68 | 7.05 | 7.39 | 7.71 | 8.32 |
| $CO_2$($H_x$×$10^{-5}$ kPa) | 0.37 | 0.8 | 1.05 | 1.24 | 1.44 | 1.66 | 1.88 | 2.12 | 2.36 | 2.60 | 2.87 | 3.46 |

$$H_c = \frac{H_x M_{solvent}}{1000\rho}$$

Fig.1. Schematic of photocatalytic $CO_2$ reduction and $H_2O$ splitting in the twin reactor.

Fig.2. $H_2$ and $O_2$ production during photocatalytic reduction of pure $CO_2$ with simultaneous $H_2O$ splitting.

Fig.3. $CH_3OH$ production during photocatalytic reduction of pure $CO_2$ with simultaneous $H_2O$ splitting.

Fig.4. $CH_3CHO$ and $HCOOCH_3$ production during photocatalytic reduction of pure $CO_2$ with simultaneous $H_2O$ splitting.

Fig.5. $CH_3OH$ concentration at the CO to $CO_2$ ratio of 1:10.

Fig.6. $CH_3OH$ concentration at the CO to $CO_2$ ratio of 1:5.

Fig.7. $H_2$, $O_2$ and $CH_3OH$ concentrations with the pure CO as the reactant gas.

Fig.8. Total $CH_3OH$ concentration, $C_xH_3OH$ and $C_yH_3OH$ concentrations at the CO to $CO_2$ ratio of 1:10.

Fig.9. Total $CH_3OH$ concentration, $C_xH_3OH$ and $C_yH_3OH$ concentrations at the CO to $CO_2$ ratio of 1:5.

Fig.10. $CH_3CHO$ concentrations at various CO to $CO_2$ gas mixture ratios.

Fig.11. $CH_3OH$ concentration change with time at various pressures.

Fig.12. $CH_3OH$ concentration change with time at various temperatures.

Fig.13. Light intensity distribution in $CO_2$ reduction reactor. (a) 8:00, (b) 12:00, (c) 16:00.

Fig.14. Average light intensity change over time under the sun light.

Fig.15. Concentration changes of $H_2$, $O_2$ and $CH_3OH$ over time under the sun light.

Fig.16. Reaction rate changes of water splitting and $CO_2$ reduction over time under the sun light.

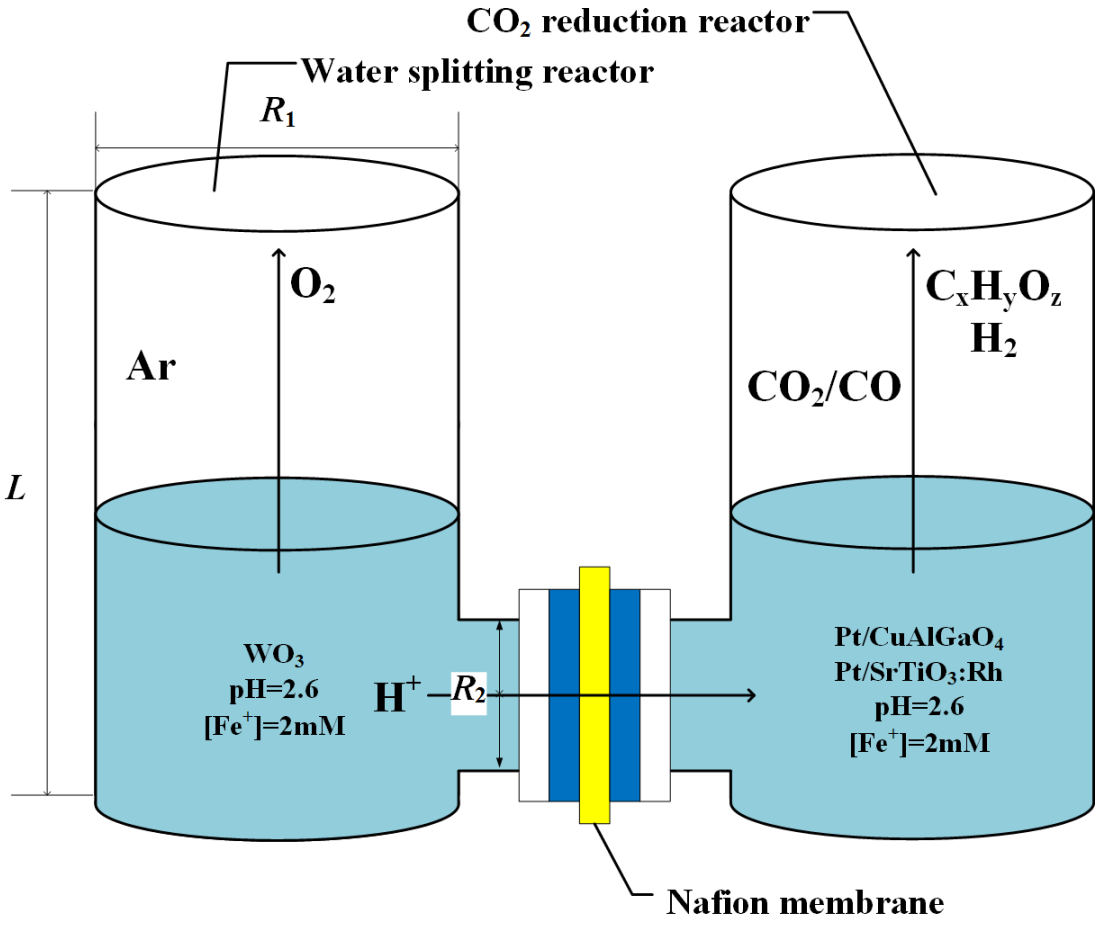
CO2 reduction reactor
Water splitting reactor
R1
O2
Ar
L
CxHyOz
H2
CO2/CO
WO3
pH=2.6
[Fe+]=2mM
H+
R2
Pt/CuAlGaO4
Pt/SrTiO3:Rh
pH=2.6
[Fe+]=2mM
Nafion membrane

Fig.1.

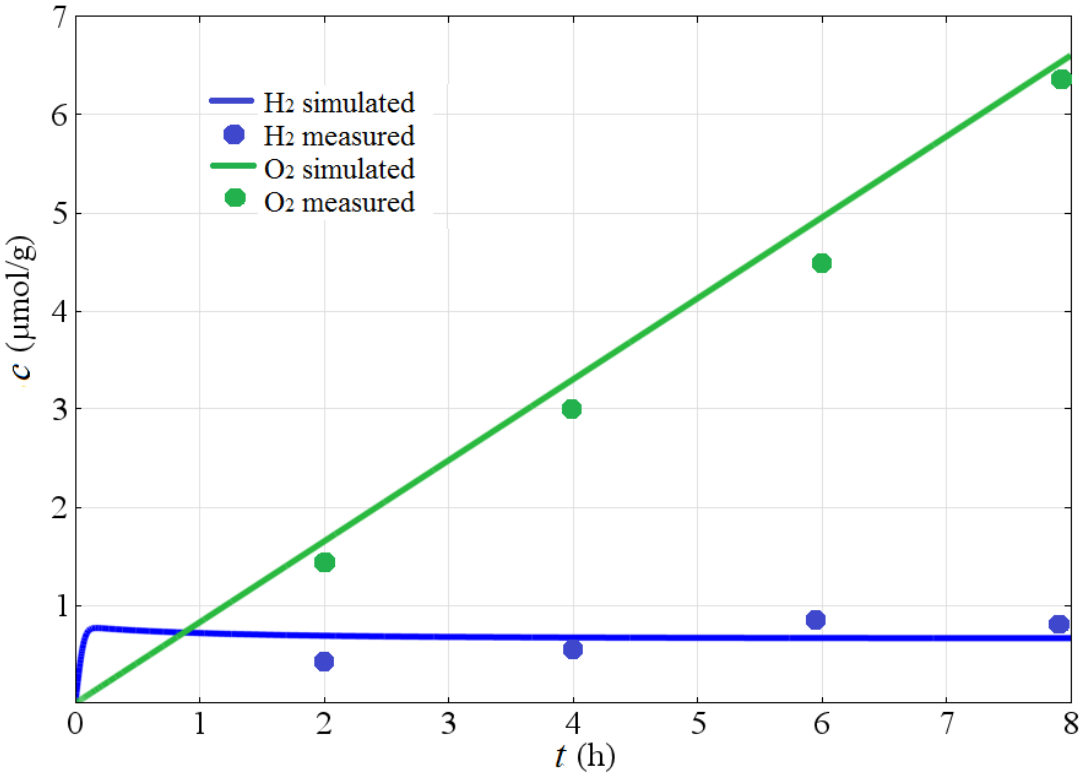
H2 simulated
H2 measured
O2 simulated
O2 measured
c (μmol/g)
t (h)
0
1
2
3
4
5
6
7
8

Fig.2.

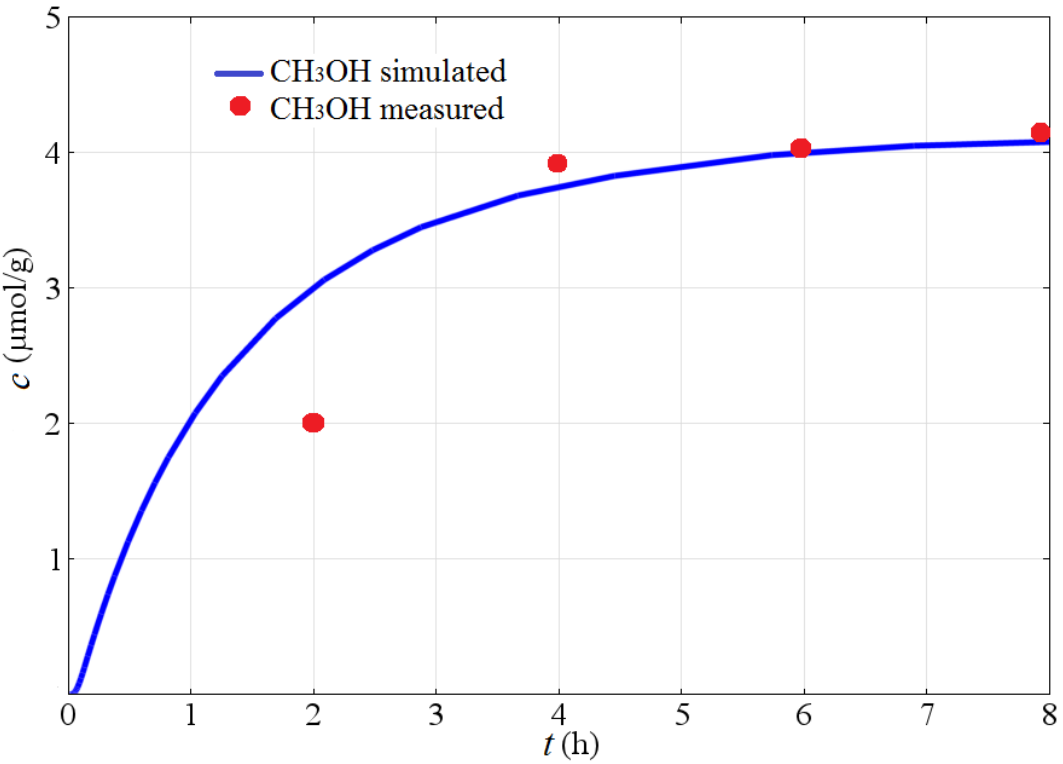


Fig.3.

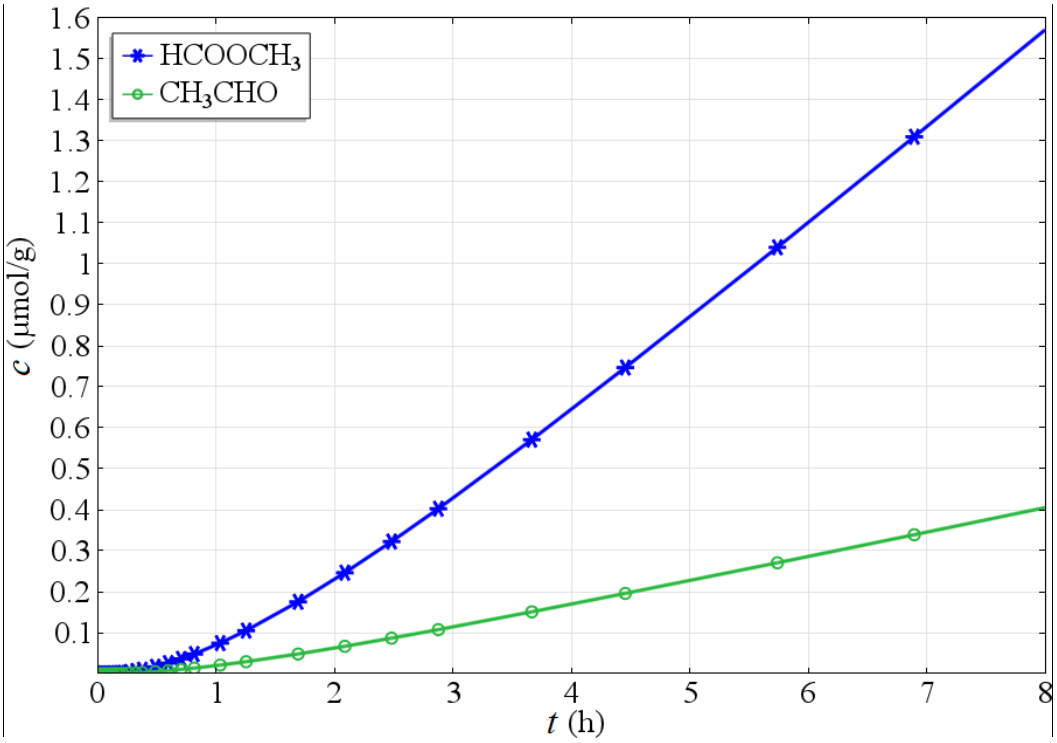
HCOOCH3
CH3CHO
c (μmol/g)
t (h)
1.6
1.5
1.4
1.3
1.2
1.1
1
0.9
0.8
0.7
0.6
0.5
0.4
0.3
0.2
0.1
0
1
2
3
4
5
6
7
8

Fig.4.

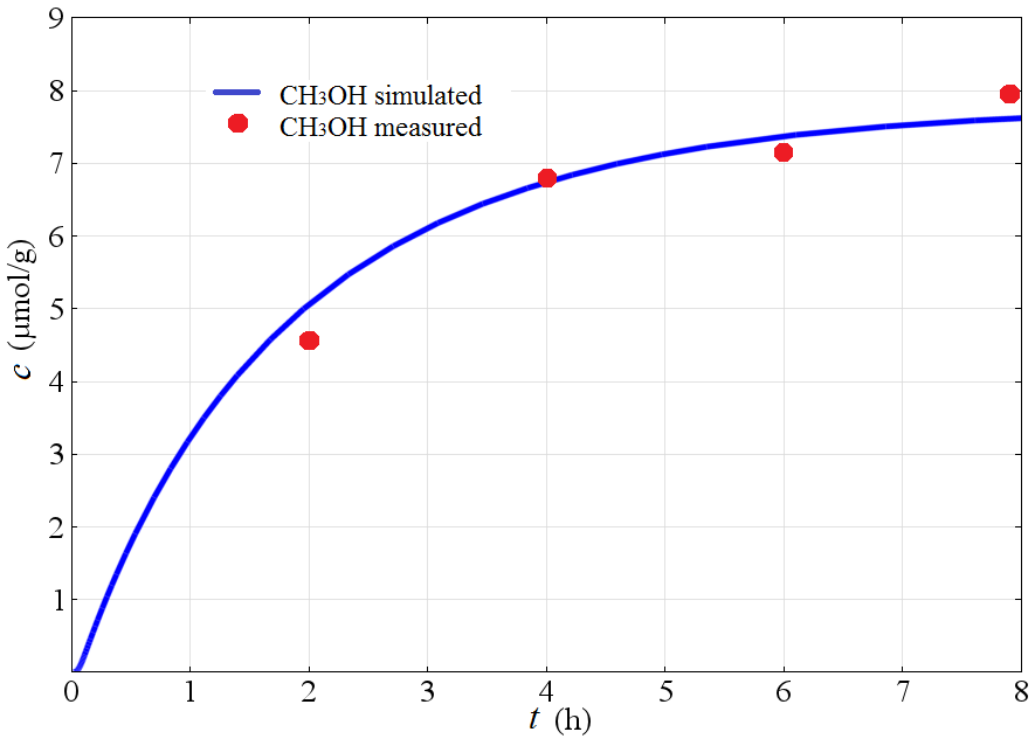


Fig.5.

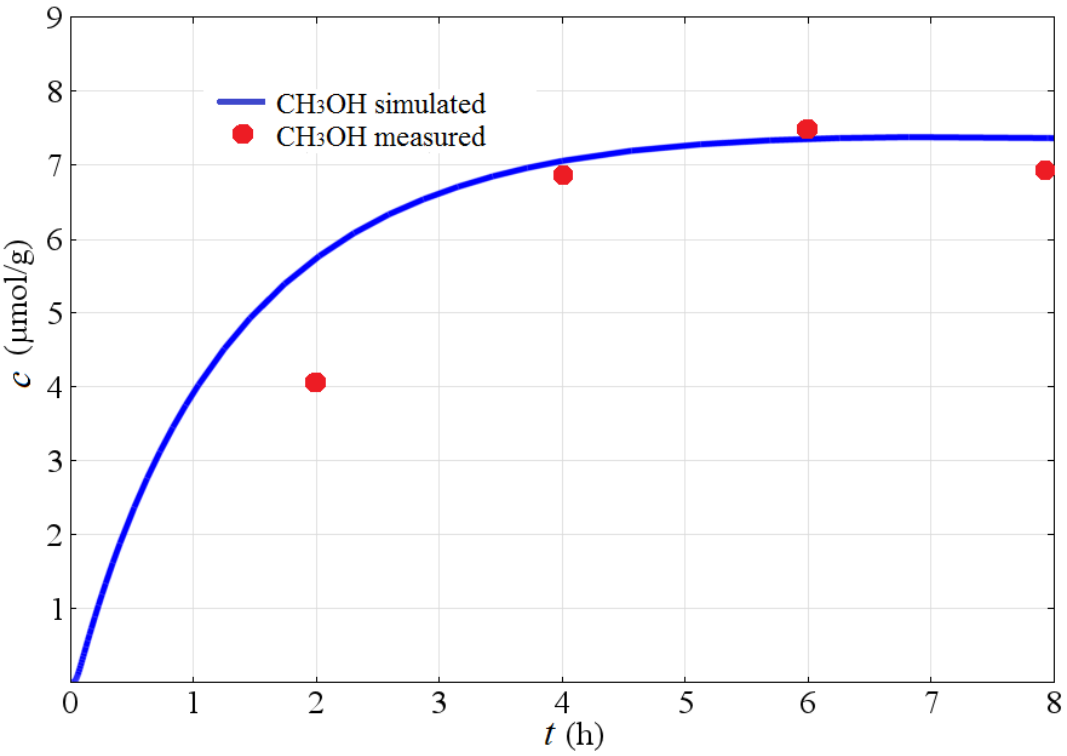


Fig.6.

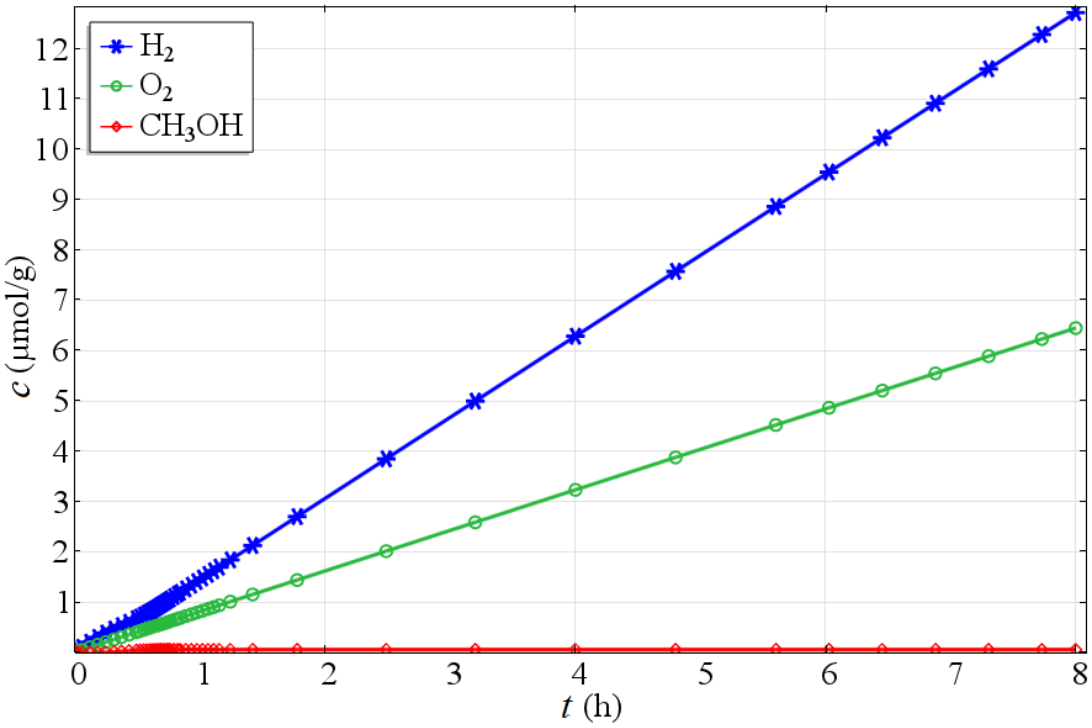


Fig.7.

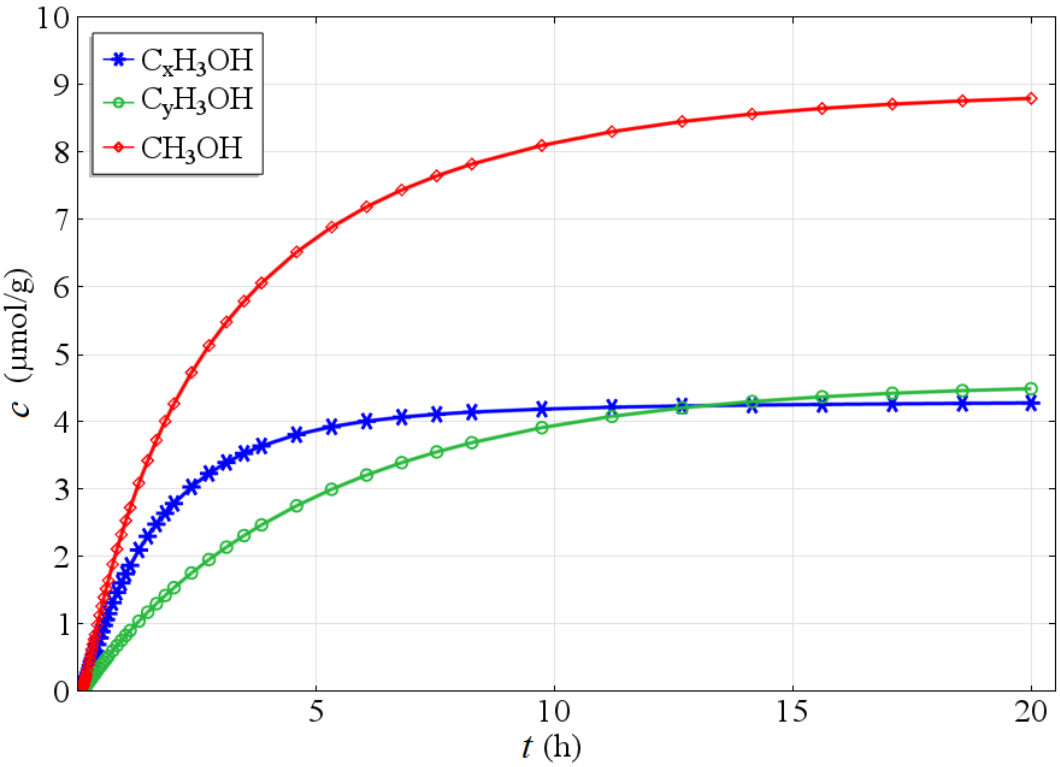


Fig.8.

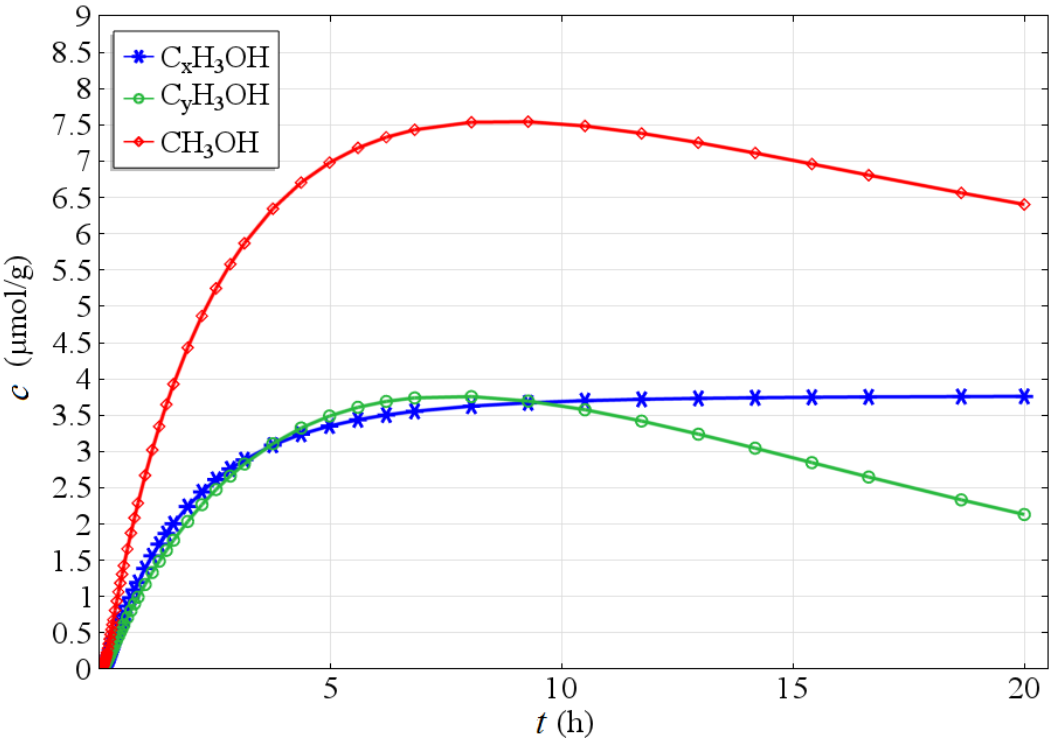
$C_xH_3OH$
$C_yH_3OH$
$CH_3OH$
c (μmol/g)
t (h)
0
0.5
1
1.5
2
2.5
3
3.5
4
4.5
5
5.5
6
6.5
7
7.5
8
8.5
9
5
10
15
20

Fig.9.

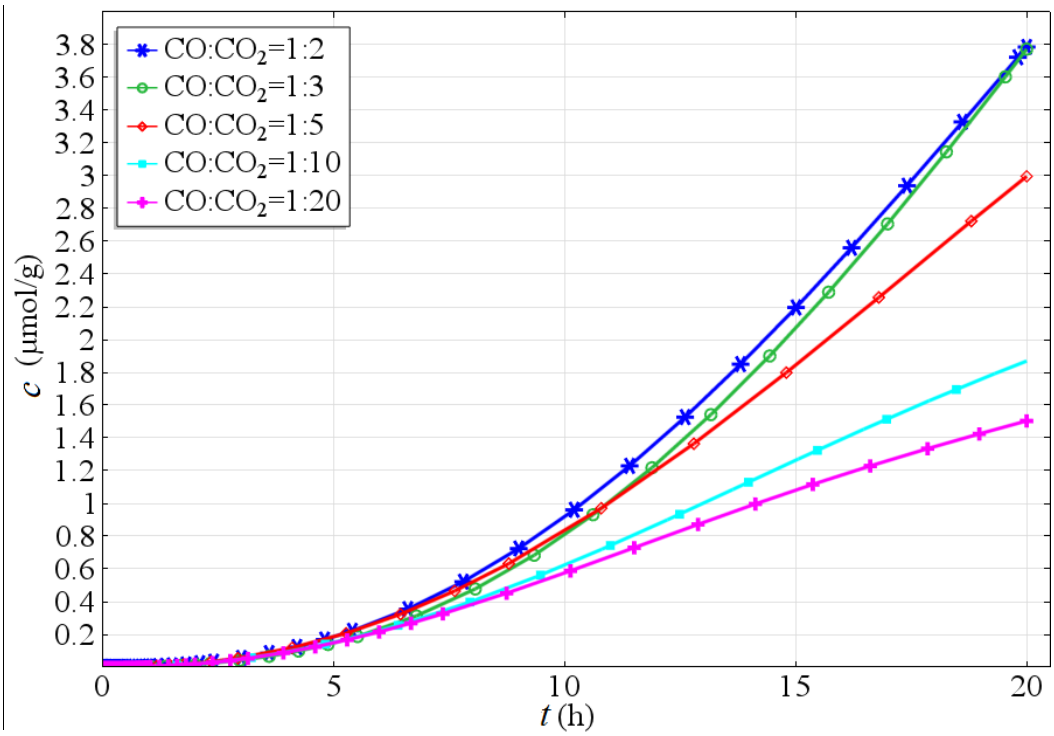
CO:CO2=1:2
CO:CO2=1:3
CO:CO2=1:5
CO:CO2=1:10
CO:CO2=1:20
c (μmol/g)
t (h)
0
5
10
15
20
0.2
0.4
0.6
0.8
1
1.2
1.4
1.6
1.8
2
2.2
2.4
2.6
2.8
3
3.2
3.4
3.6
3.8

Fig.10.

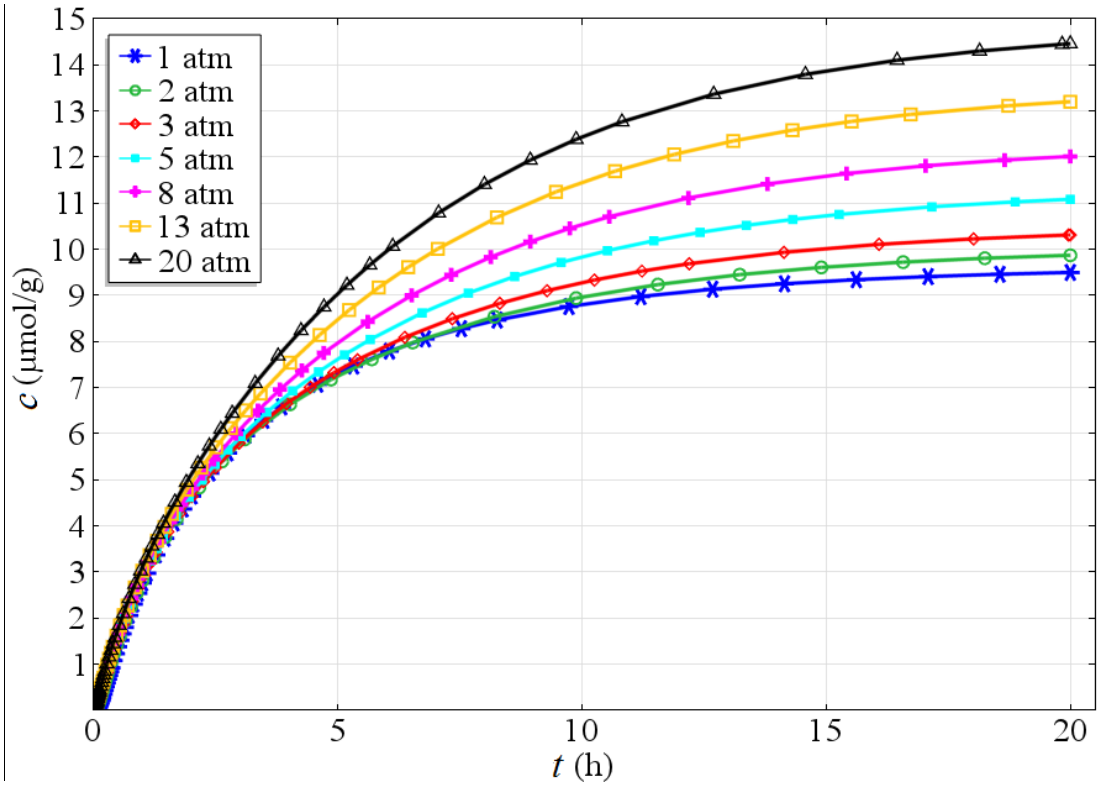
1 atm
2 atm
3 atm
5 atm
8 atm
13 atm
20 atm
c (μmol/g)
t (h)
0
5
10
15
20
1
2
3
4
5
6
7
8
9
10
11
12
13
14
15

Fig.11.

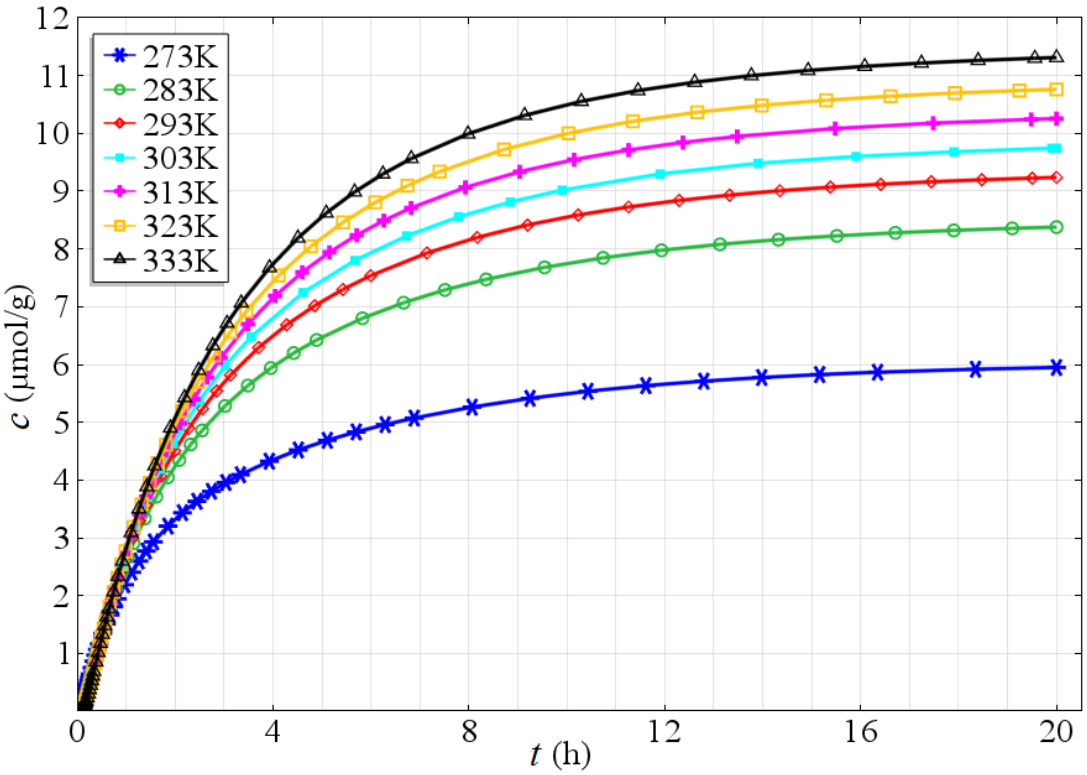
273K
283K
293K
303K
313K
323K
333K
c (μmol/g)
t (h)
0
4
8
12
16
20
1
2
3
4
5
6
7
8
9
10
11
12

Fig.12.

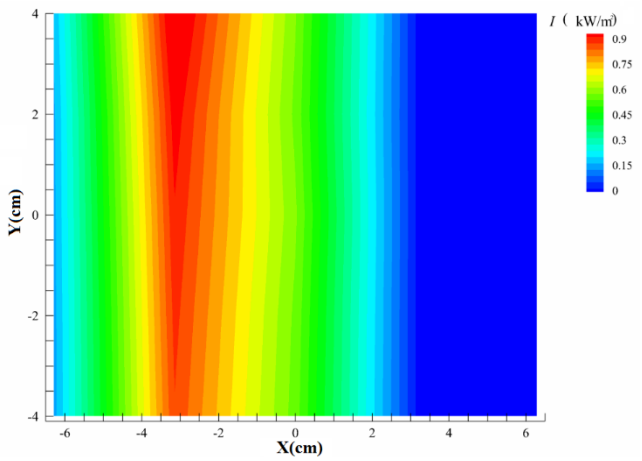
I ( kW/m²)
0.9
0.75
0.6
0.45
0.3
0.15
0
Y(cm)
X(cm)

(a)

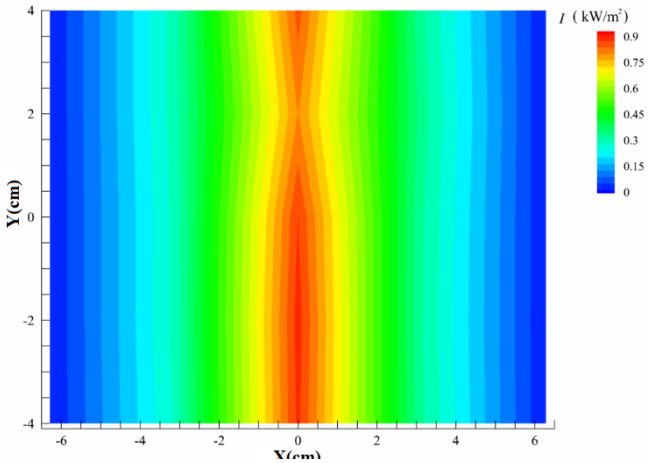
I ( kW/m²)
0.9
0.75
0.6
0.45
0.3
0.15
0
Y(cm)

(b)

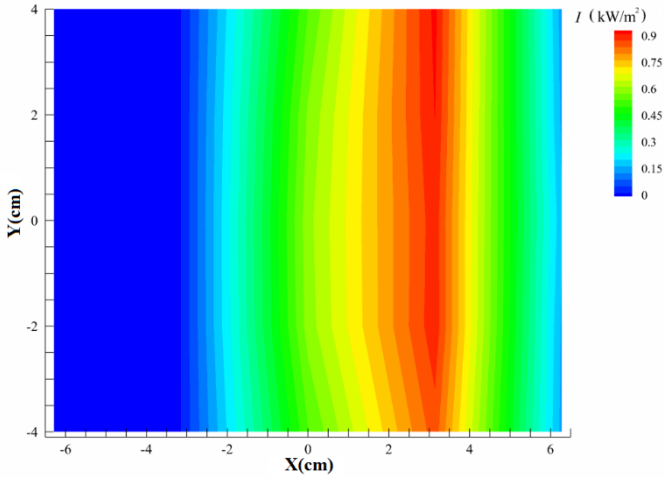
I ( kW/m²)
0.9
0.75
0.6
0.45
0.3
0.15
0
Y(cm)
X(cm)

(c)

Fig.13.

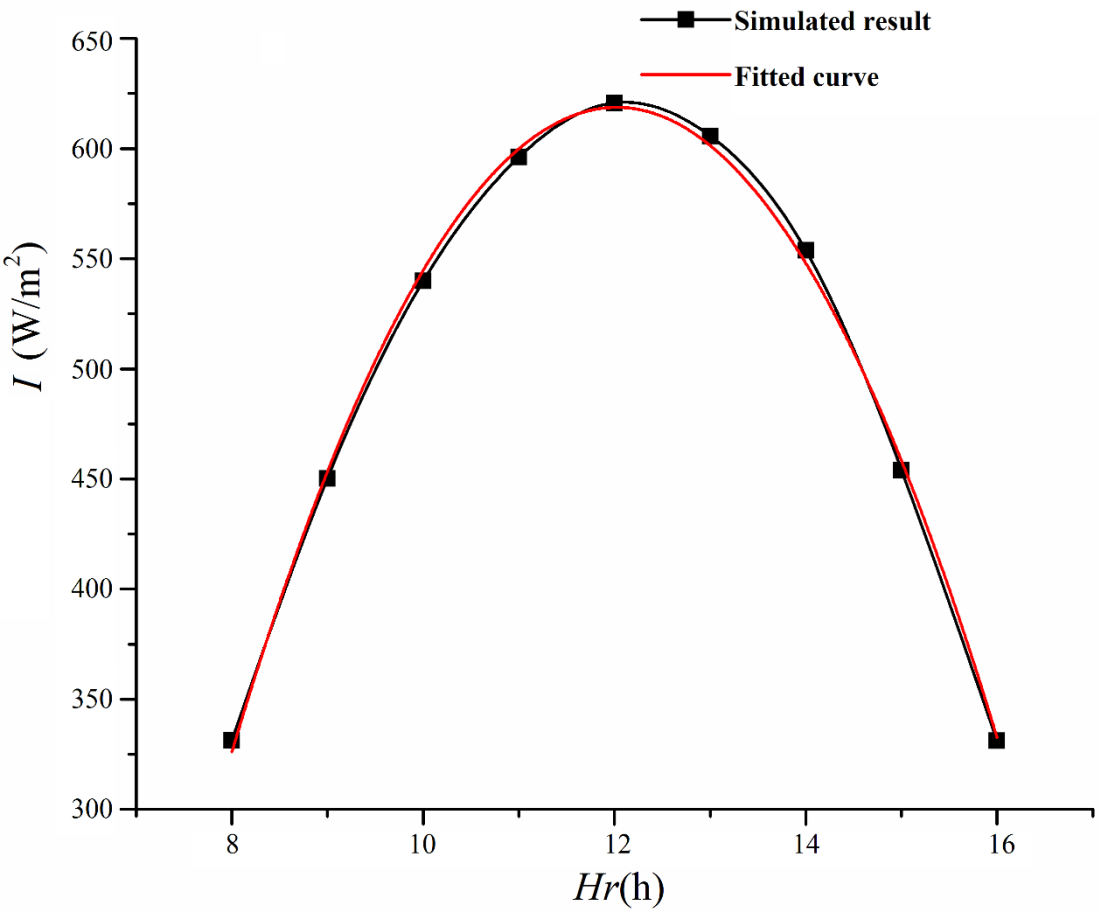
Simulated result
Fitted curve
650
600
550
500
450
400
350
300
I (W/m2)
8
10
12
14
16
Hr(h)

Fig.14.

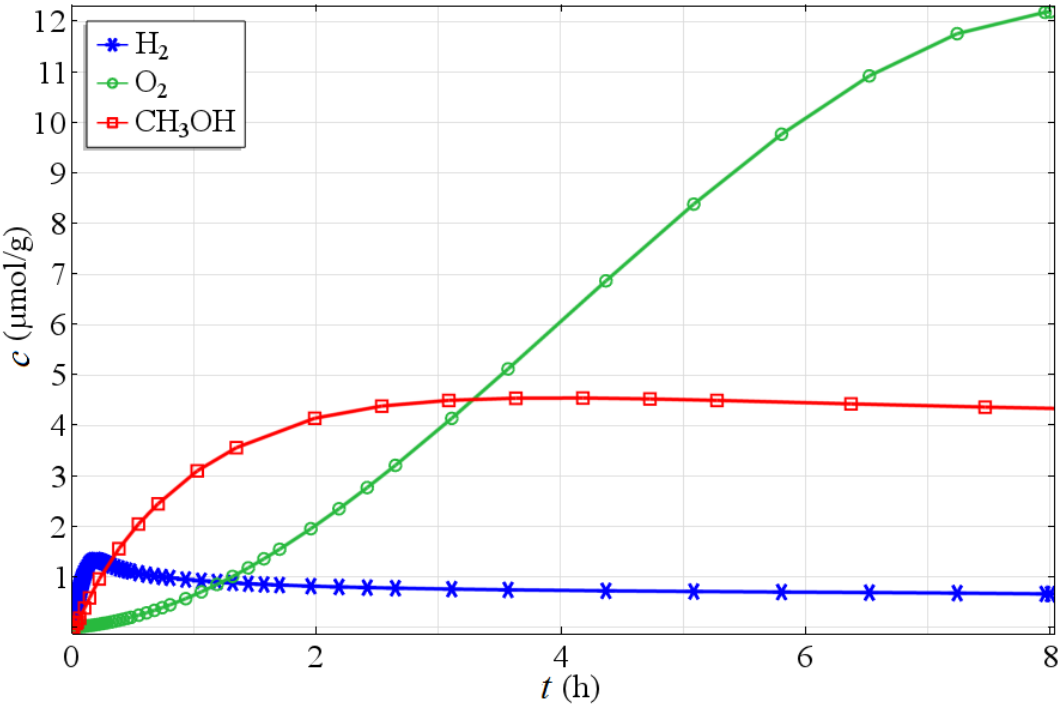


Fig.15.

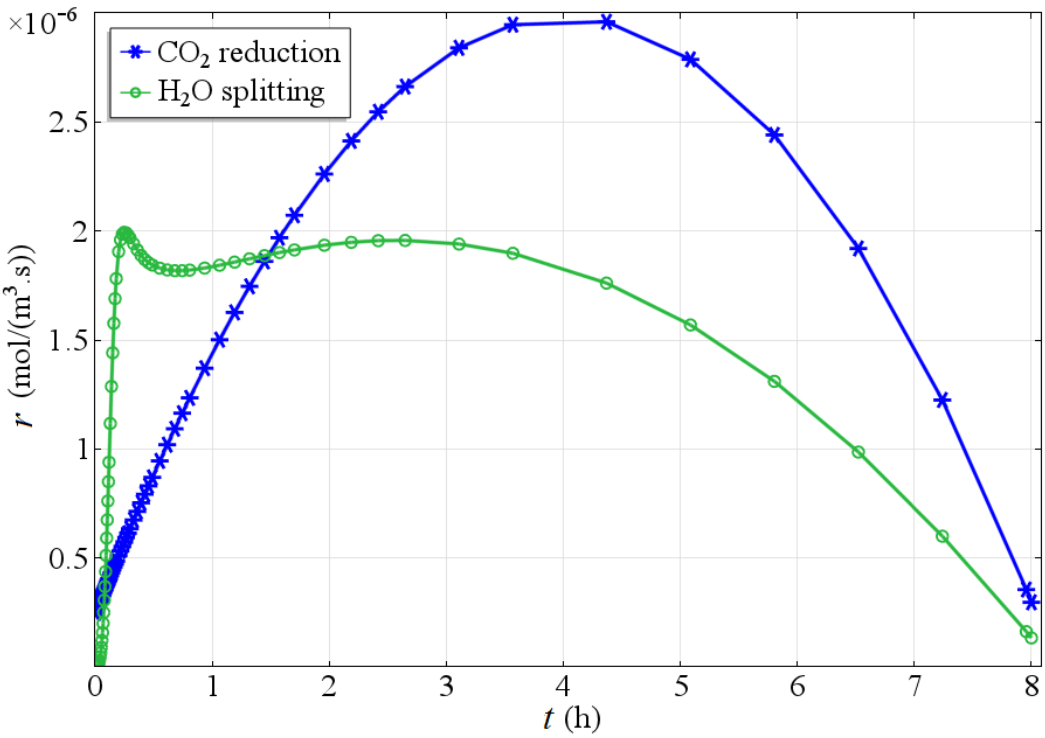
×10^-6
CO2 reduction
H2O splitting
r (mol/(m^3.s))
t (h)
0
0.5
1
1.5
2
2.5
0
1
2
3
4
5
6
7
8

Fig.16.